OPEN ACCESS

Original research

Targeting squalene epoxidase restores anti-PD-1 efficacy in metabolic dysfunction-associated steatohepatitis-induced hepatocellular carcinoma

Jun Wen ,[1] Xiang Zhang ,[1] Chi Chun Wong,[1] Yating Zhang,[1] Yasi Pan,[1] Yunfei Zhou,[1] Alvin Ho-Kwan Cheung,[2] Yali Liu,[1] Fenfen Ji,[1] Xing Kang,[1] Dabin Liu,[1] Jun Yu [1]

► Additional supplemental material is published online only. To view, please visit the journal online (https://doi.org/10.1136/gutjnl-2023-331117).

[1]Institute of Digestive Disease and Department of Medicine and Therapeutics, State Key Laboratory of Digestive Disease, Li Ka Shing Institute of Health Sciences, CUHK Shenzhen Research Institute, The Chinese University of Hong Kong, Hong Kong SAR, China
[2]Department of Anatomical and Cellular Pathology, The Chinese University of Hong Kong, Hong Kong SAR, China

Correspondence to
Dr Jun Yu, Department of Medicine and Therapeutics, The Chinese University of Hong Kong, Hong Kong SAR, China; junyu@cuhk.edu.hk

Received 11 September 2023
Accepted 29 April 2024

To cite: Wen J, Zhang X, Wong CC, *et al*. *Gut* Epub ahead of print: [*please include* Day Month Year]. doi:10.1136/gutjnl-2023-331117

ABSTRACT

Objective Squalene epoxidase (SQLE) promotes metabolic dysfunction-associated steatohepatitis-associated hepatocellular carcinoma (MASH-HCC), but its role in modulating the tumour immune microenvironment in MASH-HCC remains unclear.

Design We established hepatocyte-specific *Sqle* transgenic (tg) and knockout mice, which were subjected to a choline-deficient high-fat diet plus diethylnitrosamine to induce MASH-HCC. SQLE function was also determined in orthotopic and humanised mice. Immune landscape alterations of MASH-HCC mediated by SQLE were profiled by single-cell RNA sequencing and flow cytometry.

Results Hepatocyte-specific *Sqle* tg mice exhibited a marked increase in MASH-HCC burden compared with wild-type littermates, together with decreased tumour-infiltrating functional IFN-γ^+ and Granzyme B$^+$ CD8$^+$ T cells while enriching Arg-1$^+$ myeloid-derived suppressor cells (MDSCs). Conversely, hepatocyte-specific *Sqle* knockout suppressed tumour growth with increased cytotoxic CD8$^+$ T cells and reduced Arg-1$^+$ MDSCs, inferring that SQLE promotes immunosuppression in MASH-HCC. Mechanistically, SQLE-driven cholesterol accumulation in tumour microenvironment underlies its effect on CD8$^+$ T cells and MDSCs. SQLE and its metabolite, cholesterol, impaired CD8$^+$ T cell activity by inducing mitochondrial dysfunction. Cholesterol depletion in vitro abolished the effect of SQLE-overexpressing MASH-HCC cell supernatant on CD8$^+$ T cell suppression and MDSC activation, whereas cholesterol supplementation had contrasting functions on CD8$^+$ T cells and MDSCs treated with SQLE-knockout supernatant. Targeting SQLE with genetic ablation or pharmacological inhibitor, terbinafine, rescued the efficacy of anti-PD-1 treatment in MASH-HCC models.

Conclusion SQLE induces an impaired antitumour response in MASH-HCC via attenuating CD8$^+$ T cell function and augmenting immunosuppressive MDSCs. SQLE is a promising target in boosting anti-PD-1 immunotherapy for MASH-HCC.

WHAT IS ALREADY KNOWN ON THIS TOPIC

⇒ Metabolic dysfunction-associated steatohepatitis-induced hepatocellular carcinoma (MASH-HCC) is an emerging malignancy with few therapeutic options.
⇒ MASH-HCC harbours an immunosuppressive tumour microenvironment.

WHAT THIS STUDY ADDS

⇒ Squalene epoxidase (SQLE), a rate-limiting enzyme in cholesterol biosynthesis, plays a critical role in shaping the tumour immune microenvironment of MASH-HCC, as revealed by immunological profiling of transgenic mice with liver-specific SQLE overexpression or knockout.
⇒ SQLE drives immunosuppression through the inactivation of cytotoxic CD8$^+$ T cells together with the simultaneous induction of immunosuppressive function of myeloid-derived suppressor cells (MDSCs).
⇒ Mechanistically, we discovered that cholesterol, a downstream metabolite of SQLE, is responsible for the concomitant CD8$^+$ T cells suppression and activation of MDSCs.
⇒ Repurposing of terbinafine, an Food and Drug Administration-approved drug targeting SQLE, synergises with anti-PD-1 therapy to suppress the growth of MASH-HCC in mouse models.

HOW THIS STUDY MIGHT AFFECT RESEARCH, PRACTICE OR POLICY

⇒ Targeting SQLE is a potential therapeutic strategy for promoting immune checkpoint inhibitor therapy efficacy in MASH-HCC.
⇒ SQLE inhibitors could be repurposed for MASH-HCC treatment.

INTRODUCTION

Metabolic dysfunction-associated steatotic liver disease (MASLD), considered the hepatic manifestation of metabolic syndrome, affects >25% of the global adult population and follows a rapidly rising trajectory.[1] A portion of MASLD patients develop metabolic dysfunction-associated steatohepatitis (MASH), a severe form of MASLD,[2] which could progress to cirrhosis and hepatocellular carcinoma (HCC). MASLD is an emerging risk factor of HCC, especially in developed societies.[3] MASH-HCC pathogenesis involved a cascade of

events encompassing lipotoxicity, chronic inflammation, hepatic fibrosis and culminating in tumourigenesis.[4 5] However, there is no specific treatment for MASH-HCC, and effective targeting of MASH-HCC is an unmet need.

In recent years, immune checkpoint inhibitors (ICIs) have emerged as one of the most promising strategies in cancer therapy. ICIs targeting programmed cell death protein 1 (PD-1) have been approved for the treatment of advanced HCC, with overall response rates ranging from 7% to 36%.[6 7] In contrast to the responsiveness of viral-associated HCC to ICI therapies, whether MASH-HCC responds to ICIs remains far from certain. Two studies[8 9] suggested that MASH-HCC responded poorly to ICIs in both human patients and murine models. Meanwhile, a recent meta-analysis of eight randomised controlled trials (RCTs) showed that non-viral HCC might benefit from ICI-based therapies.[10] Compared with viral-associated HCC, MASH-HCC harbours a unique tumour immune microenvironment (TIME) with accumulation of an exhausted T cell subset ($CD8^+$ $PD\text{-}1^+$), which necessitates the development of molecular targets that boost responsiveness to ICI therapies tailored to this subset of HCC patients. Nevertheless, the in-depth mechanisms underlying the immunosuppressive TIME of MASH-HCC remain poorly understood.

Squalene epoxidase (SQLE), as a rate-limiting enzyme in cholesterol synthesis, was the top upregulated metabolic gene in MASH-HCC patients.[11] Our previous work established SQLE as an oncogenic factor in MASH-HCC by driving HCC cell proliferation. However, whether or how SQLE might regulate the TIME of MASH to promote MASH-HCC is unknown. In this study, we explored the immunomodulatory role of SQLE in MASH-HCC and evaluated SQLE as a potential therapeutic target for improving anti-PD-1 efficacy. Characterisation of immune landscape in liver-specific *Sqle* transgenic (*Sqle* tg) and knockout mice harbouring MASH-HCC revealed that SQLE is pivotal in impairing effective immune surveillance through the inhibition of cytotoxic T cell function while simultaneously inducing immunosuppressive activity of myeloid-derived suppressor cells (MDSCs). Mechanistically, we demonstrated that SQLE enriches cholesterol in the TIME, which in turn, directly antagonises effector T cells while activating MDSCs. Finally, we showed that targeting SQLE by gene knockout or repurposing of SQLE inhibitor (Terbinafine) could restore the efficacy of anti-PD-1-based immunotherapy for MASH-HCC.

METHODS

Mouse models and treatments

Hepatocyte-specific *Sqle* tg or knockout mice were constructed by Biocytogen (Beijing, China) as described previously.[11 12] Hepatocyte-specific *Sqle* tg or knockout male mice and their wild-type (WT) littermates received a single intraperitoneal (i.p.) injection of diethylnitrosamine (DEN) (5 mg/kg) at 2 weeks of age, and then placed on choline-deficient, high-fat diet (CDHFD) (Research Diets, New Brunswick, New Jersey, USA) to induce MASH-HCC.[13] At the indicated time point, mice were randomised into different treatment groups. Terbinafine (80 mg/kg) or phosphate buffered saline (PBS) (vehicle) was given through oral gavage daily for a total of 7 weeks. Anti-PD-1 antibody (clone RMP1-14, BioXCell) or IgG2a control (clone 2A3, BioXCell) was given via i.p. injection (200 µg/mouse), biweekly for 3 weeks. At the endpoint, the livers were harvested, and the number of hepatic tumours was counted. Tumour load of individual mouse liver was calculated with the following formula: the sum of mean diameters of all tumours in each mouse; mean diameter=(major diameter+minor diameter)/2.[14]

To establish an orthotopic mouse model of MASH-HCC, C57BL/6 male mice at the age of 6 weeks were fed CDHFD for 20 weeks before intrahepatic injection, and CDHFD was continued till the end of the experiment. Murine RIL-175 cells with or without *Sqle* knockout (1×10^6 cells) or Hepa1-6 cells (2×10^6 cells) with or without *Sqle* overexpression were suspended in 10 µL in a 5:5 solution of PBS and Matrigel (Corning) and injected into the left lobe of mouse liver. These cells carried the luciferase reporter (pLenti-EF1a-luciferase-CMV-GFP-P2A-Puro), which enabled weekly bioluminescence imaging to monitor tumour growth after luciferin injection (150 mg/kg, i.p., Promega). Mice were sacrificed at 3 weeks postintrahepatic injection. To deplete $CD8^+$ T cells, mice were injected with a single dose of 400 µg (i.p.) anti-mouse CD8α antibody (clone 2.43, BioXCell) or IgG2b control (clone LTF-2, BioXCell), followed by 200 µg doses every 3 days for 15 days. To eliminate MDSCs, mice were injected i.p. with 200 µg anti-mouse Ly6G/Ly6C (Gr-1) antibody (clone RB6-8C5, BioXCell) or IgG2b control (clone LTF-2, BioXCell) every other day for 16 days. Tumours were measured according to the following formula: (major diameter)×(minor diameter)^2/2.

Humanised mouse model

NOD.Cg-*Prkdc*^{scid} *Il2rg*^{tm1Wjl}/SzJ (NSG) mice aged 3–5 weeks were subjected to sublethal body gamma irradiation (150–170 cGy/mouse). After 24 hours, they were intravenously administered with 8×10^4 human cord blood $CD34^+$ haematopoietic stem cells (STEMCELL) via the tail vein. The engraftment of human $CD45^+$ cells in humanised $CD34^+$ mice was monitored at the 16th and 20th week after transplantation by flow cytometric analysis on the proportions of human $CD45^+$ cells in mouse peripheral blood via the tail incision. Mice with human $CD45^+$ cells accounting for >25% of the total of human and mouse $CD45^+$ cells were available for the following experiments. Subsequently, the established humanised mice were subcutaneously injected with human MASH-HCC cell line HKCI2 cells (1×10^7 cells in 100 µLl in a 50:50 solution of PBS and Matrigel). Three weeks after subcutaneous injection, mice were randomly divided into two groups, namely PBS and terbinafine. Terbinafine (80 mg/kg) or PBS (vehicle) was given through oral gavage daily till the endpoint. Tumour sizes were measured every 3 days. Tumour volume was measured with the following formula: (major diameter)×(minor diameter)^2/2.

Statistical analysis

Statistical analysis was performed using GraphPad Prism V.9 (GraphPad Software). All results were presented as mean±SEM. To compare the data between two groups, Mann-Whitney U test or Student's t-test with or without Welch's correction was employed. To compare the difference among three or more groups with two factors, a two-way analysis of variance with multiple comparisons within each column or row was used. A two-tailed $p<0.05$ was considered statistically significant.

Additional methods are provided in online supplemental file 1.

RESULTS

Hepatocyte-specific *Sqle* knockin suppresses $CD8^+$ T cell effector function but promotes MDSC immunosuppressive function in murine MASH-HCC.

To explore the role of SQLE in regulating antitumour immunity, we first established a MASH-HCC mouse model induced

by CDHFD plus DEN single injection in hepatocyte-specific *Sqle* tg mice and WT littermates (figure 1A). Western blot and immunohistochemistry staining confirmed the overexpression of Sqle in the livers of *Sqle* tg mice (online supplemental figure S1A). *Sqle* tg mice demonstrated elevated serum α-fetoprotein levels, increased tumour multiplicity and burden as compared with WT littermates (figure 1B). Histological examination confirmed HCC development accompanied by key features of MASH, including hepatocyte ballooning and inflammatory cell infiltration (figure 1C). To evaluate the effect of SQLE overexpression on the TIME, we performed flow cytometry analysis of MASH-HCC tumours (figure 1D). We did not observe significant differences with regard to the overall intratumoural levels of $CD4^+$ T cells, $CD8^+$ T cells, NK cells, NKT cells, macrophages or MDSCs (online supplemental figure S1B and figure 1H). Notably, flow cytometry of functional T cell markers demonstrated that both tumours and non-tumourous hepatic tissues of *Sqle* tg mice displayed reduction of IFN-γ^+ and Granzyme B^+ $CD8^+$ T subsets (figure 1E,F), together with remarkable induction of PD-1, tumour necrosis factor-α (TNF-α) and CXCR6 in intratumoural $CD8^+$ T cells (figure 1G), consistent with phenotypes of pathogenic $CD8^+$ T cells contributing to MASH and MASH-HCC progression.[8 15] Intratumoural T cells are known to be antagonised by MDSCs.[16] Whereas there was no significant alteration in MDSC levels between *Sqle* tg and WT groups (figure 1H), arginase-1^+ (Arg-1^+) MDSCs were increased in *Sqle* tg mice (figure 1I), suggesting that tumour-infiltrating MDSCs in *Sqle* tg mice had elevated immunosuppressive activity.

To decipher the functional alterations of intratumoural T cells in *Sqle* tg mice, we next performed single-cell RNA sequencing (scRNA-seq) of intratumoural $CD45^+$ leucocytes to comprehensively document the immune landscape (figure 1D). Unsupervised clustering unravelled 25 clusters, among which 11 major clusters were annotated based on the expression of known markers (online supplemental figure S1C).[17 18] We further reclustered T cells and identified six subclusters, of which $CD8^+$ T cell was the predominant cell cluster (online supplemental figure S1D). Comparison of $CD8^+$ T cells from WT and *Sqle* tg tumours revealed that the latter expressed lower levels of genes associated with effector function (*Gzma*, *Gzmb*, *Ifng*, *Cst7* and *Prf1*), but with the increased expression of exhaustion markers (*Tnfrsf9*, *Pdcd1*, *Havcr2*, *Tigit*, *Cd244a*, *Lag3* and *Tox*), as well as proinflammatory genes (*Ccl3* and *Tnf*) (figure 1J). Consistent with these observations, gene set enrichment analysis revealed that genes involved in T cell receptor signalling in $CD8^+$ T cells were highly depleted in *Sqle* tg mice compared with WT mice (figure 1K). In addition, gene set variation analysis showed that metabolic pathways such as oxidative phosphorylation and amino acid metabolism were downregulated in $CD8^+$ T cells from *Sqle* tg mice, which could limit their proliferation and effector function[19] (figure 1L). GO enrichment analysis further validated that genes related to mitochondrial function were downregulated in $CD8^+$ T cells from *Sqle* tg mice (figure 1M). Collectively, these results indicate that hepatic SQLE overexpression impairs $CD8^+$ T cell effector function and augments immunosuppressive activity of MDSCs in murine MASH-HCC.

SQLE depletion potentiates antitumour immune response in orthotopic and spontaneous MASH-HCC models

To validate our results in *Sqle* tg mice, we constructed an orthotopic MASH-HCC mouse model through intrahepatic injection of murine RIL-175 cells with or without *Sqle* knockout into the MASH liver in mice induced by CDHFD (figure 2A and online supplemental figure S2A). *Sqle* knockout attenuated the growth of orthotopic tumours, as evidenced by significantly suppressed luciferase signals, tumour weight and tumour volume of *Sqle* knockout tumours compared with sgNC tumours (figure 2B,C). Flow cytometry showed that *Sqle* knockout tumours had increased infiltration of IFN-γ^+ and Granzyme B^+ $CD8^+$ T cells (figure 2D), as well as a marked reduction in Arg-1^+ MDSCs (figure 2E). To validate the function of SQLE in the TIME of spontaneous MASH-HCC, we next established hepatocyte-specific *Sqle* knockout mice and initiated MASH-HCC using DEN plus CDHFD (figure 2F and online supplemental figure S2B). *Sqle* knockout significantly reduced tumour number and load compared with WT littermates (figure 2G). Moreover, we observed increased functional cytotoxic $CD8^+$ T cells and reduced immunosuppressive MDSCs in *Sqle* knockout mice (figure 2H,I), consistent with that in orthotopic MASH-HCC. Together, our results indicate that *Sqle* deletion augmented antitumour immunity by promoting effector $CD8^+$ T cells and diminishing immunosuppressive function of MDSCs, culminating in reduced MASH-HCC growth.

Targeting SQLE with terbinafine boosts antitumour immunity in mice with humanised immune system

To confirm the role of SQLE in modulating human antitumour immune response in human MASH-HCC, human $CD34^+$ haematopoietic stem cells were used to establish humanised immune system in immunodeficient NSG mice (figure 2J).[20] Mice with peripheral blood mononuclear cells (PBMCs) comprising >25% human $CD45^+$ cells were available for subsequent tumour inoculation (figure 2J). Human MASH-HCC HKCI2 cells were subcutaneously injected. To diminish SQLE in vivo, we repurposed terbinafine, a highly effective and selective inhibitor targeting SQLE (online supplemental figure S2C).[11] We observed that terbinafine significantly suppressed tumour volume and tumour weight in humanised mice compared with the vehicle group (figure 2K,L). Next, we also analysed the TIME in HKCI2 tumour tissues by flow cytometry (figure 2M). Inhibition of SQLE led to a profound increase in IFN-γ^+ and Granzyme B^+ $CD8^+$ T cells (figure 2N), demonstrating our finding based on multiple mouse models that silencing SQLE potentiates antitumour immune response in MASH-HCC. Along with the increased infiltration of cytotoxic $CD8^+$ T cells, terbinafine reduced Arg-1^+ MDSC accumulation (figure 2O). Thus, pharmacological inhibition of SQLE using terbinafine is an effective approach to enhance antitumour immunity to suppress MASH-HCC growth in mice with humanised immune system.

Tumour-intrinsic SQLE downregulates $CD8^+$ T cell effector function

To determine if tumour-intrinsic SQLE directly impairs cytotoxic T cell function, we treated T cells isolated from human PBMCs with the conditioned medium of MASH-HCC cells with SQLE overexpression or knockout (in HKCI10 or HKCI2 cells, respectively) (figure 3A). In line with our in vivo findings, the proportion of IFN-γ^+ and Granzyme B^+ $CD8^+$ T cells was significantly decreased after culturing with the conditioned medium of SQLE-overexpressing HKCI10 cells (figure 3B). In contrast, the conditioned medium of SQLE-knockout HKCI2 cells exerted an opposite effect on IFN-γ and Granzyme B expression in $CD8^+$ T cells (figure 3C). In addition, consistent results were observed in murine T cells cultured with the conditioned medium from murine HCC cells (Hepa1-6 and RIL-175) with SQLE overexpression and knockout, respectively (online supplemental figure

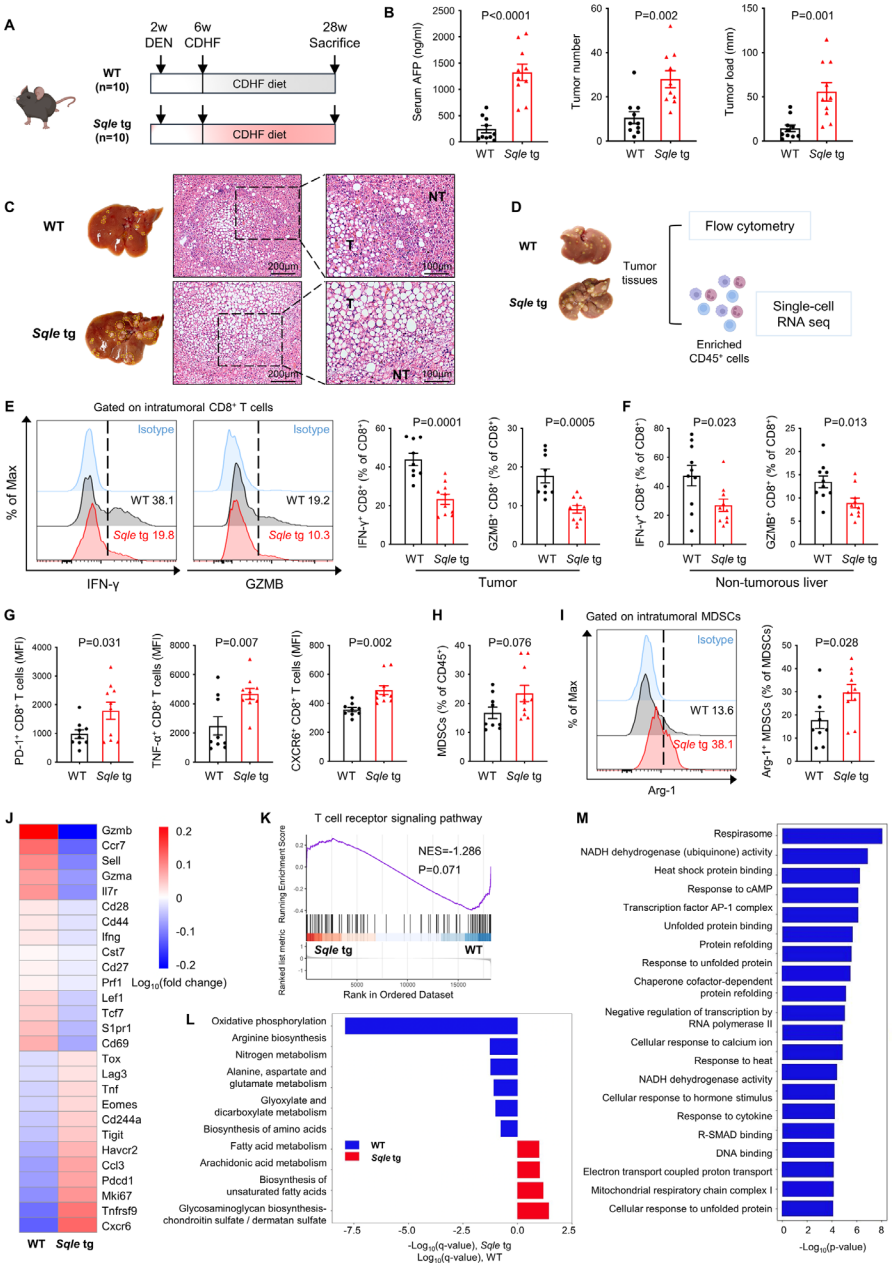

Figure 1 Hepatocyte-specific *Sqle* knockin suppresses CD8$^+$ T cell effector function but promotes MDSC immunosuppressive function in murine MASH-HCC. (A) Experimental design for DEN-injected CDHFD-induced MASH-HCC model. At 2 weeks of age, WT or *Sqle* tg mice were injected i.p. with a single dose of DEN (5 mg/kg). Mice were fed CDHFD from the ages of 6 weeks to 28 weeks. (B) Serum AFP levels, tumour number and tumour load of WT and *Sqle* tg mice. *Sqle* tg mice showed higher serum levels of AFP and developed significantly more and larger tumours compared with their WT littermates (WT n=10; *Sqle* tg n=10). (C) Representative liver images (left) and H&E staining images (right) of WT and *Sqle* tg mice. (D) Experimental design for immune cell analysis by flow cytometry and single-cell RNA-sequencing (scRNA-seq) in tumours from WT or *Sqle* tg mice. Tumour tissues from WT or *Sqle* tg mice were divided into two parts for flow cytometry and scRNA-seq. CD45$^+$ cells were enriched from tumour tissues of WT or *Sqle* tg mice by MACS, followed by scRNA-seq. (E) Flow cytometry of tumour-infiltrating IFN-γ$^+$ and Granzyme B$^+$ CD8$^+$ T cells in WT and *Sqle* tg mice (WT n=9; *Sqle* tg n=10). (F) Flow cytometry of IFN-γ$^+$ and Granzyme B$^+$ CD8$^+$ T cells in non-tumourous liver of WT and *Sqle* tg mice (WT n=10; *Sqle* tg n=10). (G) PD-1, TNF-α and CXCR6 expression on tumour-infiltrating CD8$^+$ T cells from WT and *Sqle* tg mice as shown by mean fluorescence intensity (MFI) (WT n=9; *Sqle* tg n=10). (H) Percentage of intratumoural MDSCs in WT and *Sqle* tg mice (WT n=9; *Sqle* tg n=10). (I) Flow cytometry of Arg-1$^+$ MDSCs in tumour tissues of WT and *Sqle* tg mice (WT n=9; *Sqle* tg n=10). (J) scRNA-seq data showing the expression of a curated set of gene signatures onto CD8$^+$ T cells (cluster #0 in online supplemental figure S1D) derived from WT and *Sqle* tg tumours. (K) GSEA of scRNA-seq data on CD8$^+$ T cells derived from WT or *Sqle* tg mice. A reduced trend in the enrichment of transcripts involved in T cell receptor signalling in CD8$^+$ T cells from *Sqle* tg mice compared with those from WT mice. (L) KEGG metabolic pathway enrichment analysis of scRNA-seq data on CD8$^+$ T cells derived from WT or *Sqle* tg mice. The q values of pathways enriched in *Sqle* tg and WT groups are depicted in positive and negative directions, respectively. (M) GO enrichment analysis of scRNA-seq data on CD8$^+$ T cells derived from WT or *Sqle* tg mice. The p value of gene sets downregulated in *Sqle* tg group is depicted in the positive direction. All data are shown as mean±SEM. CDHFD, choline-deficient, high-fat diet; DEN, diethylnitrosamine; GSEA, gene set enrichment analysis; MASH-HCC, metabolic dysfunction-associated steatohepatitis-associated hepatocellular carcinoma; MDSCs, myeloid-derived suppressor cells; NT, adjacent non-tumourous liver; Sqle, squalene epoxidase; T, tumour; WT, wild-type.

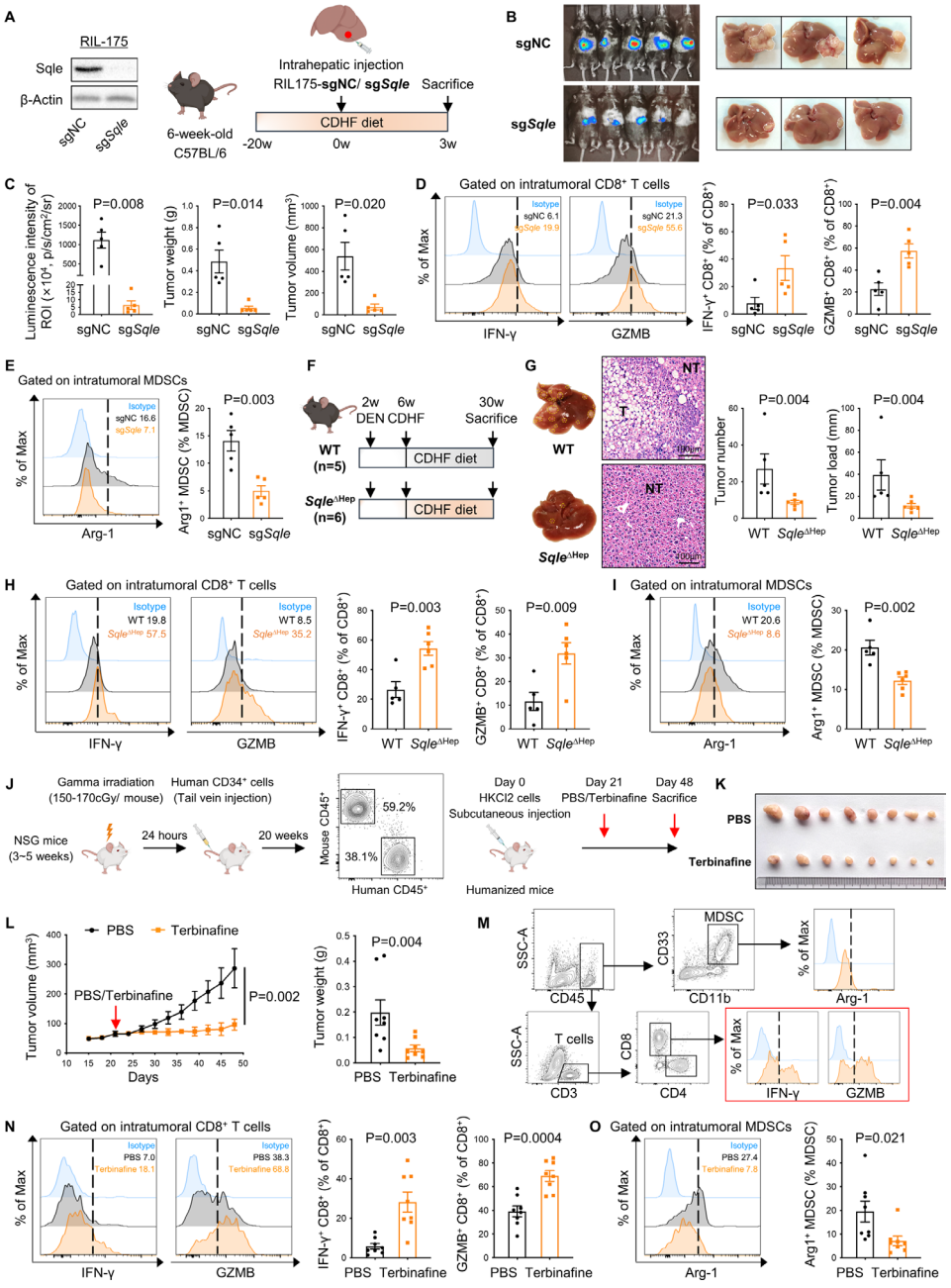

Figure 2 SQLE ablation or inhibition enhances antitumour immunity in orthotopic and spontaneous MASH-HCC mouse models and in CD34$^+$ humanised mice. (A) Experimental design of orthotopic MASH-HCC model. The underlying MASH was induced by feeding C57BL/6 mice with CDHFD for 20 weeks. Murine RIL-175 cells with or without *Sqle* knockout were injected into the left lobe of mouse liver. *Sqle* knockout in RIL-175 cells was confirmed by western blot. (B) Bioluminescent images (left) and representative liver pictures (right) of orthotopic RIL-175 tumours at the endpoint. (C) Quantification of tumour size by luminescence intensity of region of interest (ROI) (left), tumour weight (middle) and tumour volume (right) of RIL-175 orthotopic mouse model (n=5 per group). (D) Flow cytometry of tumour-infiltrating IFN-γ$^+$ and Granzyme B$^+$ CD8$^+$ T cells in RIL-175-sgNC or RIL-175-sg*Sqle* tumours (n=5 per group). (E) Flow cytometry of intratumoural Arg-1$^+$ MDSCs in RIL-175-sgNC or RIL-175-sg*Sqle* tumours (n=5 per group). (F) Experimental setup for DEN-injected CDHFD-induced MASH-HCC model using liver-specific *Sqle* knockout mice or WT littermates. (G) Representative liver images (left) and H&E staining images (middle) on WT and *Sqle* knockout livers. Liver tumour number and load (right) of WT and Sqle knockout mice (WT n=5; *Sqle*$^{\Delta Hep}$ n=6). (H) Flow cytometry of intratumoural IFN-γ$^+$ and Granzyme B$^+$ CD8$^+$ T cells in WT and *Sqle* knockout mice (WT n=5; *Sqle*$^{\Delta Hep}$ n=6). (I) Flow cytometry of tumour-infiltrating Arg-1$^+$ MDSCs in WT and *Sqle* knockout mice (WT n=5; *Sqle*$^{\Delta Hep}$ n=6). (J) Experimental setup for establishment of CD34$^+$ humanised mice (left). Percentage of human CD45$^+$ cells in PBMCs of humanised NSG mice was confirmed by flow cytometry (middle). Human MASH-HCC HKCI2 cells were subcutaneously injected into humanised mice with >25% human CD45$^+$ cells in PBMCs (right). (K) Representative images of subcutaneous tumours in PBS and terbinafine groups (n=8 per group). (L) Quantification of tumour volume (left) and tumour weight (right) in humanised mice. (M) Gating strategies of immunocytes in HKCI2 tumours of CD34$^+$ humanised mice. (N) Flow cytometry of tumour-infiltrating IFN-γ$^+$ and Granzyme B$^+$ CD8$^+$ T cells in PBS and terbinafine groups (n=8 per group). (O) Flow cytometry of Arg-1$^+$ MDSCs in subcutaneous tumours (n=8 per group). All data are shown as mean±SEM. CDHFD, choline-deficient, high-fat diet; DEN, diethylnitrosamine; MASH-HCC, metabolic dysfunction-associated steatohepatitis-associated hepatocellular carcinoma; MDSCs, myeloid-derived suppressor cells; PBMCs, peripheral blood mononuclear cells; PBS, phosphate buffered saline; SQLE, squalene epoxidase; WT, wild-type.

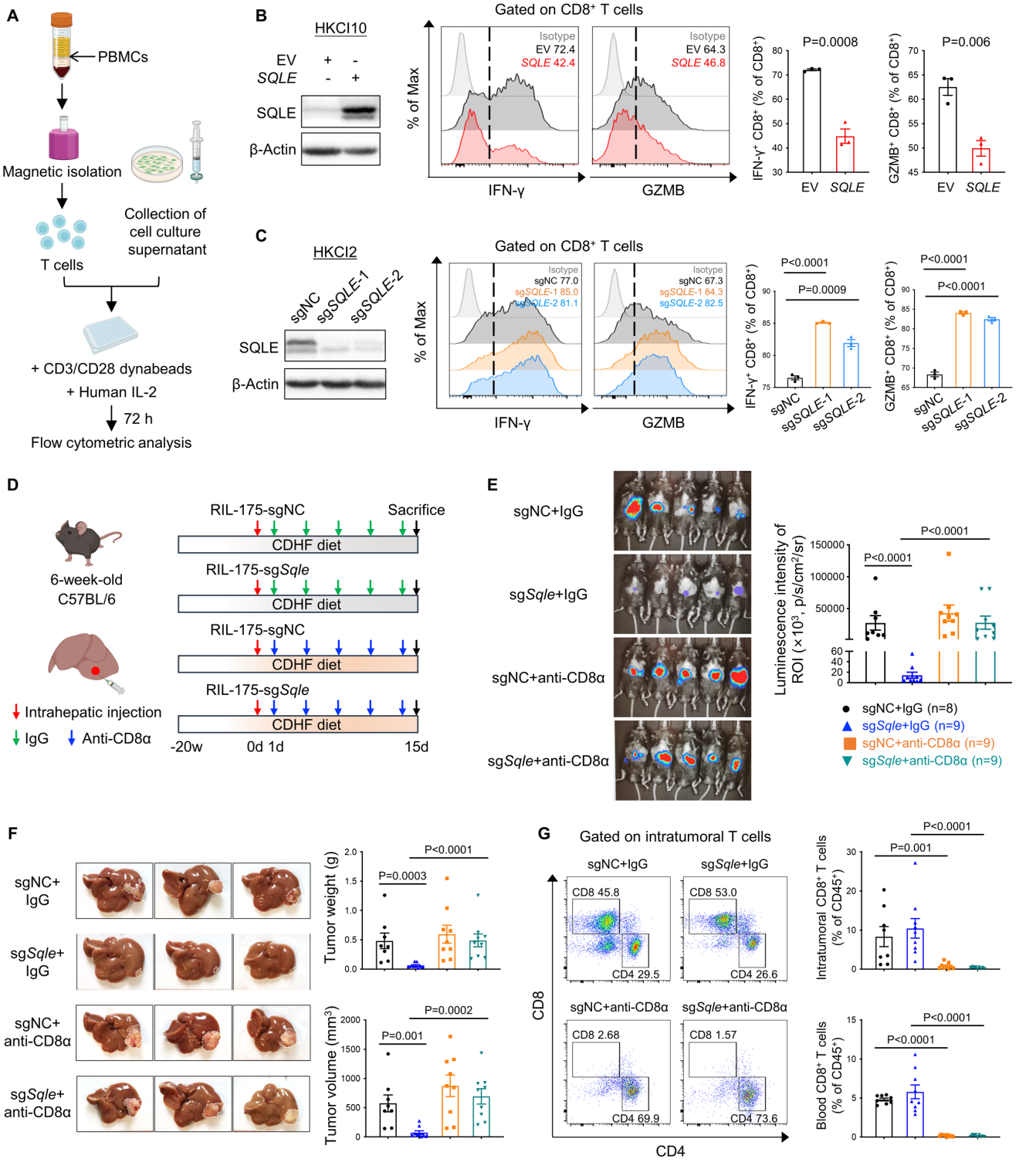

Figure 3 Tumour-intrinsic SQLE downregulates CD8$^+$ T cell effector function. (A) Experimental design for in vitro T cell co-culture assay. T cells isolated from healthy donor PBMCs were treated with indicated conditioned medium for 72 hours and analysed by flow cytometry. (B) Flow cytometry of IFN-γ$^+$ or Granzyme B$^+$ CD8$^+$ T cells treated with the conditioned medium of HCKI10 cells with or without the overexpression of SQLE. SQLE overexpression in HKCI10 cells was validated by western blot. (C) Flow cytometry of IFN-γ$^+$ or Granzyme B$^+$ CD8$^+$ T cells treated with the conditioned medium of HKCI2 with or without SQLE knockout. SQLE knockout in HKCI2 cells was validated by western blot. (D) Experimental design of orthotopic MASH-HCC mouse model with CD8$^+$ T cell depletion. RIL-175 cells with or without SQLE knockout were injected into the left lobe of mouse liver. For CD8$^+$ T cell depletion, mice were intraperitoneally injected with IgG isotype or anti-CD8α antibody (initial 400 µg followed by 200 µg per mouse, every 3 days) for 15 days. (E) Bioluminescent images and quantification of orthotopic RIL-175 tumours at the endpoint. (F) Representative images of RIL-175-sgNC or RIL-175-sg*Sqle* orthotopic tumours treated with IgG control or anti-CD8α. Tumour weight and tumour volume were quantified. (G) Depletion efficiency of CD8$^+$ T cells in orthotopic tumours and blood was confirmed by flow cytometry. Experiments were performed with three biological replicates (B,C). All data are shown as mean±SEM. CDHFD, choline-deficient, high-fat diet; MASH-HCC, metabolic dysfunction-associated steatohepatitis-associated hepatocellular carcinoma; PBMCs, peripheral blood mononuclear cells; SQLE, squalene epoxidase.

S3A–C). These results support the notion that SQLE-modulated conditioned medium of MASH-HCC cells exerts an inhibitory effect on CD8$^+$ T cell effector function.

To address whether the protumourigenic effect of SQLE was dependent on its effect on CD8$^+$ T cell-mediated antitumour immunity, we depleted CD8$^+$ T cells with anti-CD8α antibody in RIL-175 orthotopic MASH-HCC (figure 3D). In accordance with our hypothesis, the depletion of CD8$^+$ T cells abolished the tumour-inhibitory effect of SQLE knockout, as shown by bioluminescent imaging, tumour weight and tumour volume measurements (figure 3E,F). The successful depletion of CD8$^+$ T cells in the TIME and peripheral blood was confirmed by flow cytometry (figure 3G). These findings suggest that the tumour-suppressive effect of SQLE deletion was primarily dependent on potentiating the antitumour immune response of CD8$^+$ T cells.

SQLE impairs CD8$^+$ T cell effector function mainly via cholesterol accumulation

We next sought to identify the mechanisms by which SQLE provokes the immune suppression in MASH-HCC. Given that SQLE is the rate-limiting enzyme in the cholesterol biosynthesis, we hypothesised that the immunosuppressive effect of SQLE on CD8$^+$ T cells may be mediated via cholesterol. Indeed, hepatic tumour tissues derived from *Sqle* tg mice exhibited significantly higher contents of free cholesterol and cholesteryl ester compared with those from their WT littermates (figure 4A). Consistent with in vivo findings, the conditioned medium of HKCI2 cells with SQLE knockout had lower levels of free cholesterol and cholesteryl esters (figure 4B), whereas overexpression of SQLE increased total cholesterol in the conditioned medium of HKCI10 cells (figure 4C). These findings were further confirmed in orthotopic RIL-175 model, hepatocyte-specific *Sqle* knockout model and humanised mouse model (online supplemental figure S4A–C). Furthermore, we assessed de novo cholesterol biosynthesis using deuterated water (D_2O)-based isotope labelling.[21] LC-MS analysis of deuterium incorporated into cholesterol revealed decreased labelled cholesterol in SQLE-knockout cells, indicating reduced de novo cholesterol biosynthesis, whereas cholesterol biosynthesis increased in SQLE-overexpressing cells (online supplemental figure S4D,E). To ask if cholesterol is involved in SQLE-mediated immunosuppression, we supplemented cholesterol in SQLE-knockout cell conditioned medium and performed in vitro T cell co-culture (figure 4D). Cholesterol addition largely reversed SQLE knockout-induced activation of IFN-γ$^+$ and Granzyme B$^+$ CD8$^+$ T cells (figure 4E). Conversely, the addition of methyl-β-cyclodextrin (β-CD) to deplete cholesterol[22] abolished the inhibitory effect of SQLE-overexpressing conditioned medium on effector function of CD8$^+$ T cells (figure 4F). These data indicate that SQLE impairs the effector function of CD8$^+$ T cells in MASH-HCC via cholesterol accumulation.

Cholesterol exists in the circulation as free cholesterol or lipoprotein cholesterol. To ask whether it is free cholesterol or lipoprotein cholesterol is involved in modulation of CD8$^+$ T cell function, we separated conditioned medium into low (<3 kDa) and high (>3 kDa) molecular weight fractions, respectively. SQLE overexpression in HKCI10 cells increased free cholesterol and very low-density lipoproteins (VLDL/LDL) cholesterol levels (online supplemental figure S4F). In contrast, SQLE knockout in HKCI2 cells suppressed cholesterol levels in both fractions (online supplemental figure S4F), together with increased CD8$^+$ T cell function as compared with control (online supplemental figure S4G). These results imply that SQLE increased both free cholesterol and lipoprotein cholesterol to suppress CD8$^+$ T cells.

We next sought to elucidate the mechanism whereby SQLE impairs CD8$^+$ T cell function. Having shown that SQLE overexpression downregulated the expression of genes related to mitochondrial respiration pathway in CD8$^+$ T cells in the TIME of MASH-HCC (figure 1L,M), we next asked if SQLE impairs CD8$^+$ T cell activity by modulating mitochondrial function. To this end, we assessed oxygen consumption rate (OCR), spare respiratory capacity (SRC), mitochondrial membrane potential (MitoTracker Deep Red) and mitochondrial mass (MitoTracker Green) in CD8$^+$ T cells after co-culture with SQLE-overexpressing (HKCI10) or knockout (HKCI2) conditioned medium. OCR, SRC (figure 4G), mitochondrial membrane potential and mitochondrial mass (figure 4I) were downregulated in CD8$^+$ T cells treated with SQLE-overexpressing conditioned medium, and these effects were rescued by the addition of β-CD to deplete cholesterol (figure 4G,I). On the contrary, OCR, SRC (figure 4H), mitochondrial membrane potential and mitochondrial mass (figure 4J) were increased in CD8$^+$ T cells after co-culture with SQLE-knockout conditioned medium, which could be reversed by supplementation of cholesterol (figure 4H,J). Finally, we validated cholesterol as a modulator of CD8$^+$ cells, as the direct addition of cholesterol to CD8$^+$ T cells downregulated OCR, SRC, mitochondrial membrane potential and mitochondrial mass, and these effects were rescued by β-CD (online supplemental figure S4H,I). Taken together, our work has elucidated the underlying mechanism whereby SQLE and its metabolite cholesterol promote CD8$^+$ T cell dysfunction by suppressing mitochondrial function.

To validate that cholesterol biosynthesis is key for the immunomodulatory effect of SQLE, we screened downstream genes on SQLE overexpression or knockout, revealing that 24-dehydrocholesterol reductase (DHCR24) was coregulated by SQLE (online supplemental figure S4J,K). Moreover, DHCR24 phenocopied SQLE in CD8$^+$ T cell suppression. Conditioned medium from DHCR24-overexpressing HKCI2 cells inhibited CD8$^+$ T cell function, and such effects were rescued by β-CD (online supplemental figure S4L,M). In contrast, knockout of DHCR24 in HKCI10 cells reactivated CD8$^+$ T cell function, which could be abolished by cholesterol addition (online supplemental figure S4L,N). These findings suggest that the modulation of SQLE downstream enzymes involved in cholesterol biosynthesis also elicits similar effects on CD8$^+$ T cells.

Beyond its effect on cholesterol, cytokine array analysis of SQLE-knockout HKCI2 conditioned medium revealed TGF-β2 as the top downregulated cytokine (online supplemental figure S5A), and ELISA verified that SQLE promoted TGF-β2 secretion in vitro and in vivo (online supplemental figure S5B-D). As TGF-β is an inhibitory cytokine for cytotoxic T cells,[23] we investigated the contributory role of TGF-β2 on SQLE-driven CD8$^+$ T cell suppression. Antibody blockade of TGF-β2 partially abrogated CD8$^+$ T cell suppressive effect of SQLE-overexpressing HKCI10 conditioned medium (online supplemental figure S5E), whereas supplementation with recombinant TGF-β2 restored CD8$^+$ T cell suppressive effect of SQLE-knockout HKCI2 conditioned medium (online supplemental figure S5F). Hence, SQLE, at least in part, diminishes the activation of CD8$^+$ T cells by producing TGF-β2.

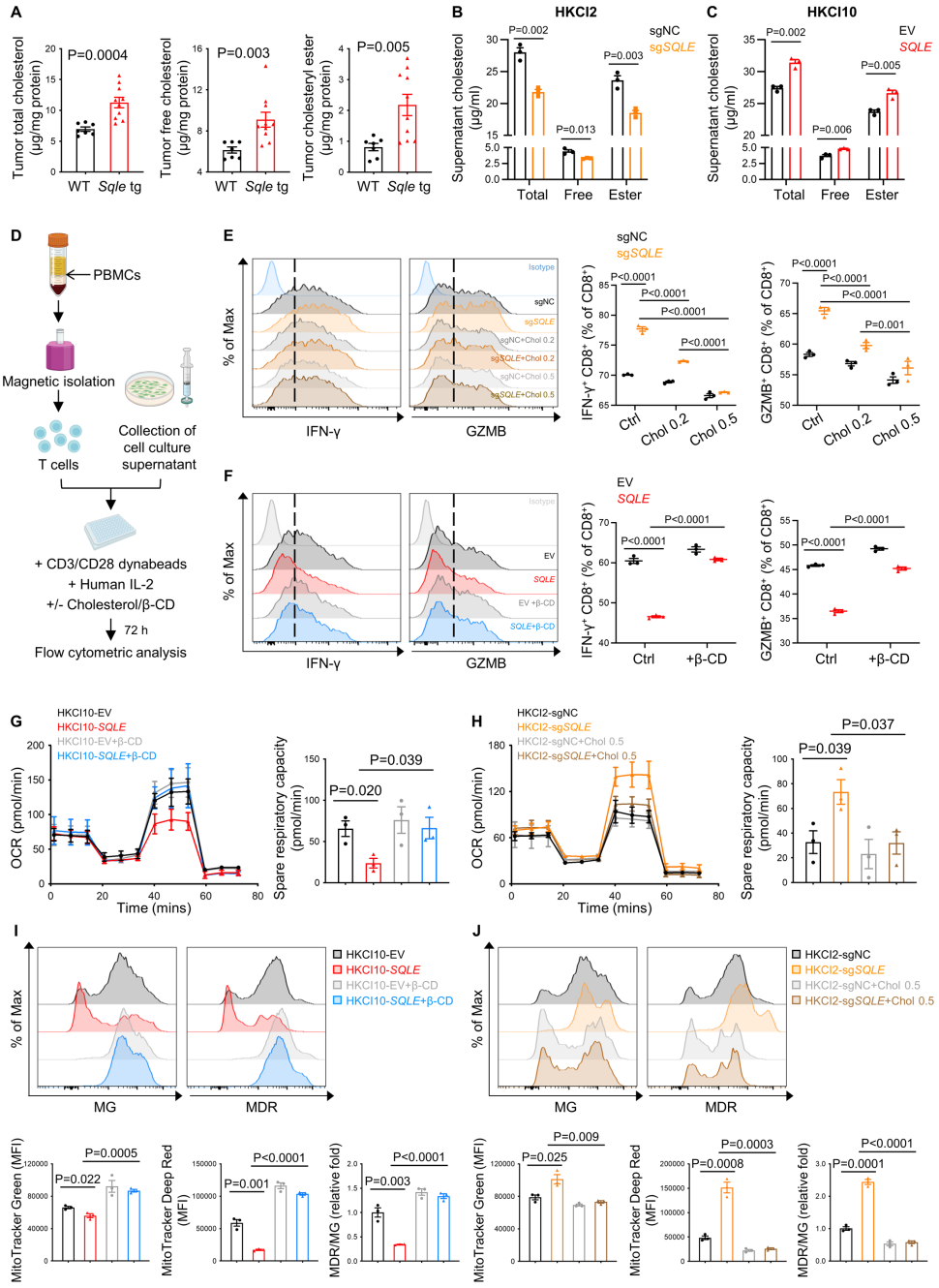

Figure 4 SQLE impairs the effector function of CD8$^+$ T cell through cholesterol accumulation. (A) Free cholesterol and cholesteryl ester concentrations in the tumours of DEN-injected CDHFD-fed MASH-HCC mice (WT n=7; *Sqle* tg n=10). (B) Cholesterol level in the conditioned medium of HKCI2 cells with or without SQLE knockout. (C) Cholesterol level in the conditioned medium of HKCI10 cells with or without SQLE overexpression. (D) Experimental design of the in vitro T cell co-culture assay. T cells isolated from healthy donor's PBMCs were treated with the indicated culture supernatants with or without the addition of cholesterol or methyl-β-cyclodextrin (β-CD) for 72 hours and were subsequently analysed by flow cytometry. (E) Isolated T cells were cultured in the conditioned medium of HKCI2-sgNC or HKCI2-sg*SQLE*, with or without addition of cholesterol. IFN-γ$^+$ and Granzyme B$^+$ CD8$^+$ T cells were determined by flow cytometry. Chol 0.2: cholesterol 0.2 μg/mL; Chol 0.5: cholesterol 0.5 μg/mL. (F) T cells were cultured in the conditioned medium of HKCI10-EV or HKCI10-*SQLE*, cells with or without β-CD (0.5 mM), followed by flow cytometry analysis. (G) Oxygen consumption rate (OCR) was measured using seahorse analysis on CD8$^+$ T cells treated with SQLE-overexpressing HKCI10 conditioned medium with or without β-CD (0.5 mM). Spare respiratory capacity (SRC) was calculated as the difference between the mean of initial OCR values and the maximal OCR values achieved after FCCP added. (H) OCR and SRC were measured using seahorse analysis on CD8$^+$ T cells treated with SQLE-knockout HKCI2 conditioned medium with or without the addition of cholesterol (0.5 μg/mL). (I) Representative histograms (upper) and MFI (down) of MitoTracker Green (MG), MitoTracker Deep Red (MDR) and the ratio of MDR to MG of CD8$^+$ T cells treated with SQLE-overexpressing HKCI10 conditioned medium with or without β-CD (0.5 mM). (J) Representative histograms (upper) and MFI (down) of MG, MDR and the ratio of MDR to MG of CD8$^+$ T cells treated with SQLE-knockout HKCI2 conditioned medium with or without the addition of cholesterol (0.5 μg/mL). Experiments were performed with three biological replicates (B,C,E–J). All data are shown as mean±SEM. CDHFD, choline-deficient, high-fat diet; DEN, diethylnitrosamine; MASH-HCC, metabolic dysfunction-associated steatohepatitis-associated hepatocellular carcinoma; PBMCs, peripheral blood mononuclear cells; SQLE, squalene epoxidase; WT, wild-type.

Tumour-intrinsic SQLE promotes immunosuppressive function of MDSCs

We next sought to identify whether SQLE also simultaneously promotes immunosuppressive function of MDSCs. To this end, we harvested CD11b$^+$ Gr-1$^+$ MDSCs from RIL-175 orthotopic MASH-HCC tumours with or without SQLE knockout (figure 5A). qPCR revealed significant downregulation of *Arg-1*, *iNOS* and *Ido-1* expression in MDSCs derived from SQLE knockout orthotopic tumours (figure 5B). Flow cytometry also validated reduced Arg-1$^+$ and iNOS$^+$ MDSCs from SQLE knockout RIL-175 tumours (figure 5C). To determine MDSC function, we performed co-culture studies of RIL-175 tumour-derived MDSCs with naïve T cells (figure 5A). Concordant with the reduced Arg-1 and iNOS levels, MDSCs from SQLE knockout tumours demonstrated remarkably diminished immunosuppressive function, as evidenced by increased IFN-γ and Granzyme B expression in CD8$^+$ T cells at 1:1 and 1:2 ratios (figure 5D). Furthermore, T cell suppression assays showed that MDSCs from SQLE knockout tumours showed attenuated capacity to suppress T cell proliferation (figure 5E). Altogether, these findings suggest that SQLE expression in MASH-HCC also drives immunosuppressive potency of MDSCs.

To determine whether the immunosuppressive activity of MDSCs contributes to SQLE-mediated MASH-HCC development, we depleted MDSCs with anti-Gr-1 antibody in Hepa1-6 orthotopic MASH-HCC (figure 5F). Depletion of MDSCs largely abrogated the tumour-promoting impact of SQLE overexpression in orthotopic MASH-HCC, as determined by bioluminescence imaging, tumour weight and tumour volume analysis (figure 5G,H). Anti-Gr-1 antibody depleted intratumoural and peripheral MDSCs, thereby reactivating functional CD8$^+$ T cells (figure 5I,J and online supplemental figure S6). This implies the protumourigenic effect of SQLE was, at least in part, dependent on MDSCs. Hence, SQLE-driven immunosuppressive MDSCs facilitate MASH-HCC development.

SQLE induces immunosuppressive activity of MDSCs via cholesterol accumulation

As cholesterol is the major metabolite generated by SQLE, we then asked whether the impact of SQLE on MDSCs involved cholesterol accumulation. To address this, we generated human MDSCs from PBMCs in vitro with the addition of GM-CSF and IL-6, and then performed co-culture assays with the conditioned medium of MASH-HCC cells (figure 6A). Whereas the proportion of Arg-1$^+$ MDSCs was suppressed by SQLE knockout, cholesterol addition restored Arg-1$^+$ MDSCs to that of control HKCI2 conditioned medium (figure 6B). Reciprocally, cholesterol depletion by β-CD abolished the induction of Arg-1$^+$ MDSCs by SQLE-overexpressing HKCI10 conditioned medium (figure 6C).

To further verify the functional significance of SQLE-stimulated MDSCs, we cultured murine MDSCs with the conditioned medium of murine MASH-HCC organoids established from WT or *Sqle* tg mice (figure 6D). Conditioned medium of *Sqle* tg organoids exerted a significant stimulatory effect on the immunosuppressive function of MDSCs, which could be reversed by cholesterol depletion with β-CD (figure 6E). Consistently, MDSCs stimulated by *Sqle* tg organoid-derived conditioned medium more strongly inhibited T cell effector function, an effect alleviated by β-CD (figure 6F,G). Our data, thus, indicate that SQLE induces the immunosuppressive activity of MDSCs in MASH-HCC via cholesterol accumulation.

Targeting SQLE rescues the efficacy of anti-PD-1 immunotherapy in MASH-HCC

Recent studies indicated that anti-PD-1 therapy is ineffective in the context of MASH-HCC.[8 9] In light of our observations that SQLE ablation could simultaneously restore effector CD8$^+$ T cell function and suppress functional MDSCs, we sought to evaluate the impact of SQLE knockout on the effectiveness of anti-PD-1 treatment in spontaneous MASH-HCC (figure 7A, online supplemental figure S7A,B). In line with previous findings, anti-PD-1 monotherapy had no effect on MASH-HCC growth (figure 7B). On the contrary, SQLE knockout markedly restored the tumour suppressive effect of anti-PD-1 (figure 7B). Moreover, proportions of tumour-infiltrating IFN-γ$^+$ and Granzyme B$^+$ CD8$^+$ T cells were increased to the highest extent in SQLE-knockout tumours treated with anti-PD-1 (figure 7C). Consistent alteration of cholesterol levels was confirmed in this therapeutic model (online supplemental figure S7C).

Next, we further tested whether pharmacological inhibition of SQLE with terbinafine could improve anti-PD-1 efficacy in mice with spontaneous MASH-HCC (figure 7D, online supplemental figure S7D,E). As expected, anti-PD-1 therapy alone could not suppress the development of MASH-HCC and even aggravated tumour formation while administration of terbinafine significantly attenuated the tumour growth (figure 7E). Moreover, the combination of terbinafine and anti-PD-1 treatment exhibited a stronger antitumour effect compared with either terbinafine or anti-PD-1 alone group (figure 7E). In addition, mice receiving the combined therapy had the highest proportion of intratumoural activated cytotoxic CD8$^+$ T cells (figure 7F). Inhibition of terbinafine on SQLE-induced cholesterol accumulation was validated in this combinational therapeutic model (online supplemental figure S7F). Taken together, we concluded that SQLE, apart from being a potential therapeutic target, could also restore anti-PD-1 efficacy against MASH-HCC in mice.

To further determine the clinical relevance of SQLE in HCC, we analysed TCGA cohort (n=371). SQLE mRNA is overexpressed in HCC tissues compared with paired adjacent normal tissues (n=50 pairs) (online supplemental figure S8A), and patients with high SQLE expression show poor survival (n=364) (online supplemental figure S8B). Further, SQLE expression positively correlates with MDSC infiltration, but negatively correlates with GZMB, a marker for effector CD8$^+$ T cells (n=371) (online supplemental figure S8C). These findings are consistent with the notion that SQLE promotes human HCC by modulating the TIME.

DISCUSSION

Our previous studies have shown that SQLE is a therapeutic target in MASH-HCC via tumour intrinsic mechanisms.[11] In this study, we further established that SQLE functions to promote an immunosuppressive TIME in MASH-HCC. MASH-HCC intrinsic SQLE drives enrichment of cholesterol, which exerts a dual action on TIME by simultaneously impairing cytotoxic CD8$^+$ T cells while promoting immunosuppressive activity of MDSCs, leading to accelerated hepatocarcinogenesis and poor response to ICI therapies. Liver-specific SQLE knockout or the pharmacological targeting of SQLE with terbinafine restored efficacy of anti-PD-1 therapy in spontaneous MASH-HCC models, corroborating SQLE as an immunotherapeutic target. Given that MASH-HCC was reported to have a very poor response to anti-PD-1-based immunotherapy,[8 9] our results have potential clinical implications for overcoming this obstacle in MASH-HCC treatment.

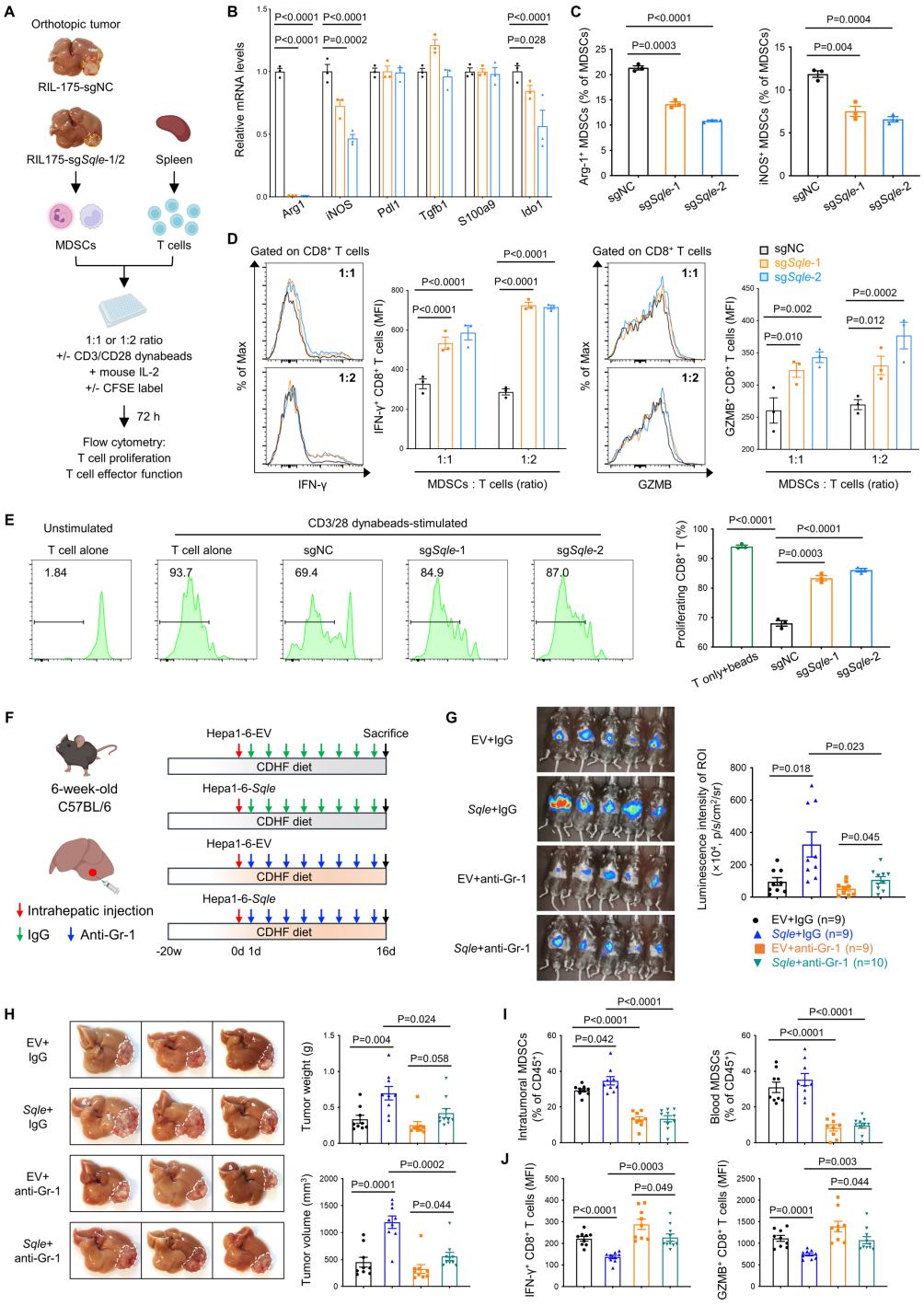

Figure 5 Tumour-intrinsic SQLE promotes immunosuppressive function of MDSCs. (A) Experimental design: Orthotopic MASH-HCC model was established using RIL-175 cells with or without SQLE knockout, and MDSCs were harvested from tumour tissues for downstream analysis. MDSCs isolated from orthotopic tumours were co-cultured with naïve T cells with or without CFSE label for 72 hours. T cells were collected for flow cytometry analysis for cell proliferation and effector function. (B) RT-qPCR analysis of MDSCs isolated from RIL-175-sgNC or RIL-175-sg*Sqle*-1/2 orthotopic tumours. (C) Flow cytometry of Arg-1$^+$ or iNOS$^+$ MDSCs in RIL-175 orthotopic tumours. (D) Flow cytometry of IFN-γ and Granzyme B expression in CD8$^+$ T cells co-cultured with MDSCs isolated from RIL-175-sgNC or RIL-175-sg*Sqle*-1/2 tumours. (E) Flow cytometry of CFSE^{low} proliferative CD8$^+$ T cells co-cultured with MDSCs (MDSCs: T cells=1:2). (F) Experimental design of orthotopic MASH-HCC model with depletion of MDSCs. Murine Hepa1-6 cells with or without SQLE overexpression were injected into the left lobe of mouse liver. For MDSC depletion, mice were intraperitoneally injected with IgG isotype or anti-Gr-1 antibody (200 µg/mouse, every other day) for 16 days. (G) Bioluminescent images and quantification of orthotopic Hepa1-6 tumours at the endpoint. (H) Representative images of Hepa1-6-EV or Hepa1-6-*Sqle* orthotopic tumours treated with IgG control or anti-Gr-1 at the endpoint (left). Tumour weight and tumour volume were quantified (right). (I) Depletion efficiency of MDSCs in orthotopic tumours and blood was confirmed by flow cytometry. (J) Levels of IFN-γ$^+$ and Granzyme B$^+$ CD8$^+$ T cells within orthotopic tumours of each group as shown by MFI. Experiments were performed with three biological replicates (B–E). All data are shown as mean±SEM. CDHFD, choline-deficient, high-fat diet; MASH-HCC, metabolic dysfunction-associated steatohepatitis-associated hepatocellular carcinoma; MDSCs, myeloid-derived suppressor cells; SQLE, squalene epoxidase.

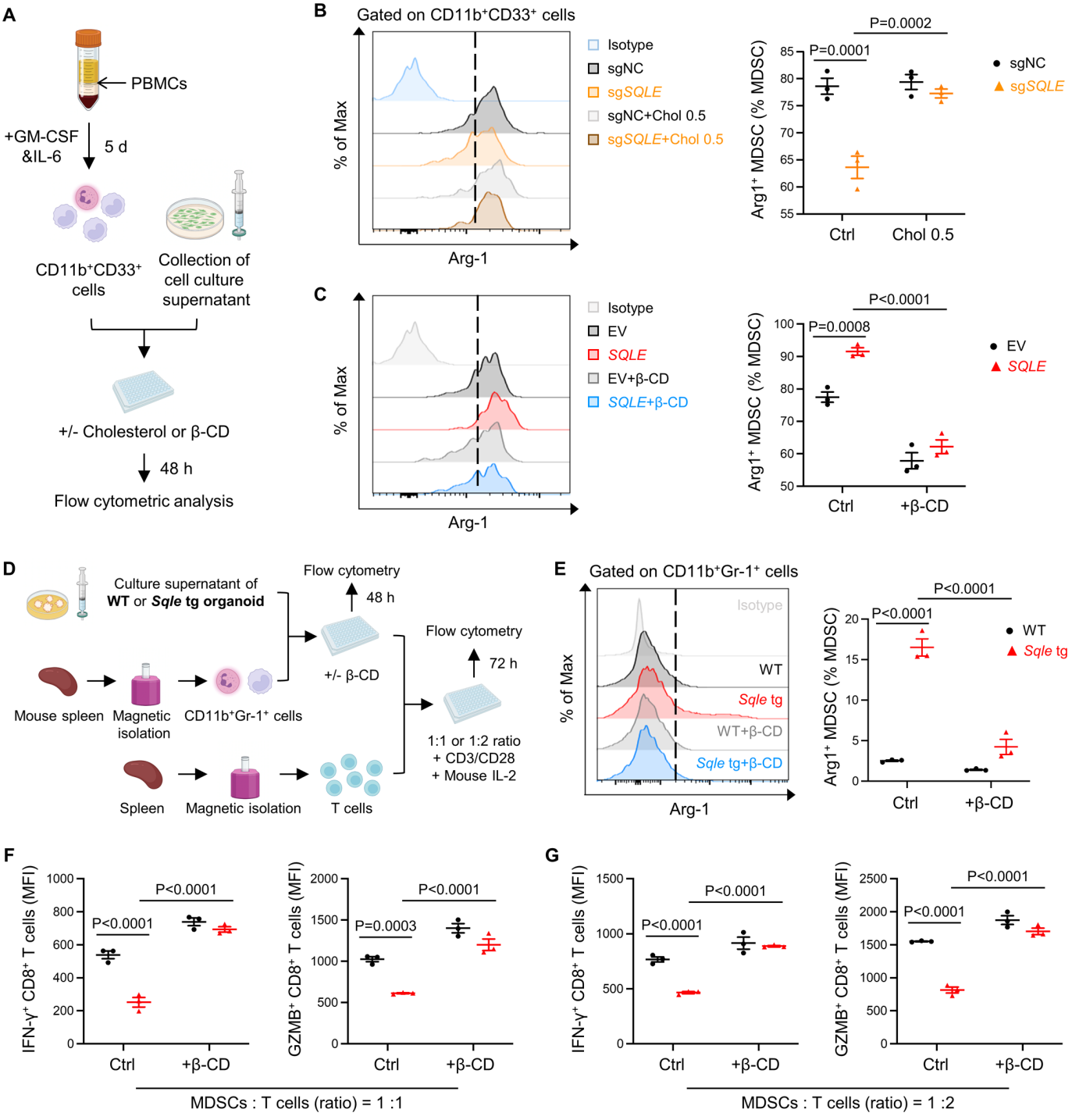

Figure 6 SQLE induces immunosuppressive activity of MDSCs via cholesterol accumulation. (A) Experimental design for inducing CD11b$^+$ CD33$^+$ cells from PBMCs and co-culture with conditioned medium. Arg-1$^+$ on MDSCs was analysed by flow cytometry. (B) Induced MDSCs were cultured in the conditioned medium of HKCI2-sgNC or HKCI2-sg*SQLE* cells with or without the addition of cholesterol (0.5 µg/mL). (C) Induced MDSCs were cultured in the conditioned medium of HKCI10-EV or HKCI10-*SQLE* cells with or without β-CD (0.5 mM). (D) Experimental design of co-culture of isolated mouse MDSCs with conditioned medium of mouse MASH-HCC organoids from WT or *Sqle* tg tumours with or without the addition of β-CD. After 48 hours, MDSCs were collected for the following function analysis by flow cytometry, or co-cultured with naïve T cells. Effector function of T cells was analysed by flow cytometry. (E) Isolated MDSCs were cultured in the conditioned medium of WT or *Sqle* tg organoids with or without β-CD (0.5 mM). The promoting effect of SQLE-overexpressing organoid supernatant on Arg-1$^+$ MDSCs was reversed by cholesterol depletion. (F, G) Levels of IFN-γ and Granzyme B on CD8$^+$ T cells co-cultured with the corresponding treated MDSCs were analysed by flow cytometry. Experiments were performed with three biological replicates (B C,E–G). All data are shown as mean±SEM. MASH-HCC, metabolic dysfunction-associated steatohepatitis-associated hepatocellular carcinoma; MDSCs, myeloid-derived suppressor cells; SQLE, squalene epoxidase; WT, wild-type.

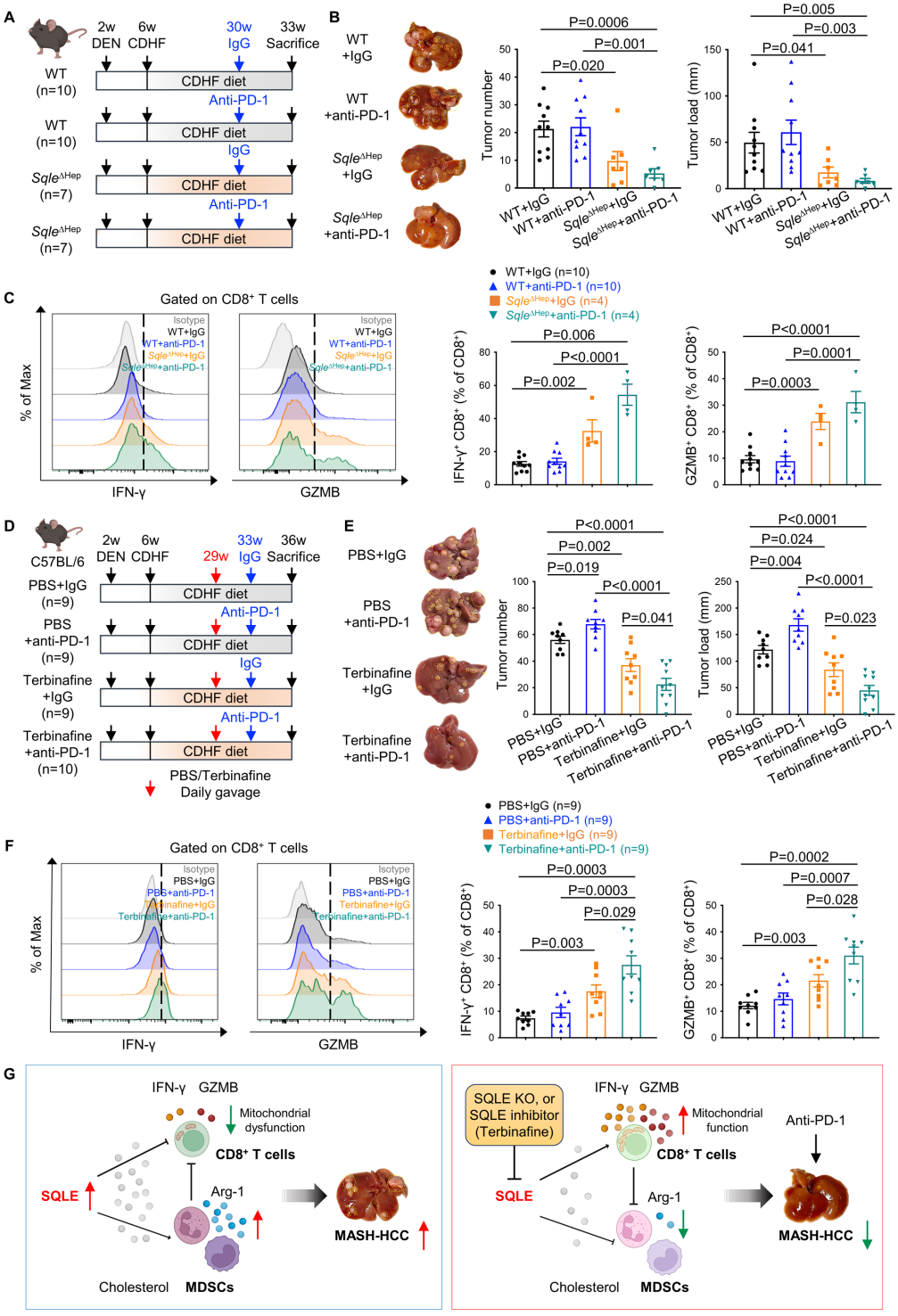

Figure 7 Targeting SQLE restores the efficacy of anti-PD-1 treatment for murine MASH-HCC. (A) Experimental design: DEN-injected CDHFD-induced MASH-HCC WT and *Sqle* knockout mice were treated with anti-PD-1 or isotype control (200 µg/mouse) biweekly for 3 weeks. (B) Representative images of the four groups (left) and endpoint assessment of tumour number and tumour load of WT or *Sqle* knockout mice treated with anti-PD-1 or IgG control (right). (C) Flow cytometry of tumour-infiltrating IFN-γ^+ and Granzyme B^+ $CD8^+$ T cells from different groups. (D) Experimental design: DEN-injected CDHFD-induced MASH-HCC mice were randomised into different treatment groups. Terbinafine (80 mg/kg) or PBS was given by oral gavage daily for 7 weeks. Anti-PD-1 antibody or IgG2a control was given via i.p. injection (200 µg/mouse), biweekly for 3 weeks. (E) Representative images of liver tumours from the four groups (left) and endpoint assessment of tumour number and tumour load (right). (F) Flow cytometry of tumour-infiltrating IFN-γ^+ and Granzyme B^+ $CD8^+$ T cells in mice from different groups. Data are shown as mean±SEM. (G) Graphical abstract. Our study demonstrated that SQLE expression in tumour cells induces an immunosuppressive microenvironment in MASH-HCC through impairing the effector function of tumour-infiltrating $CD8^+$ T cells and inducing immunosuppressive MDSCs. Targeting SQLE has the potential to reactivate cytotoxic T $CD8^+$ cells and promote anti-PD-1 therapy response in MASH-HCC. CDHFD, choline-deficient, high-fat diet; DEN, diethylnitrosamine; MASH-HCC, metabolic dysfunction-associated steatohepatitis-associated hepatocellular carcinoma; MDSCs, myeloid-derived suppressor cells; PBS, phosphate buffered saline; SQLE, squalene epoxidase; WT, wild-type.

A series of in vivo models have enabled to evaluate the function of MASH-HCC intrinsic SQLE in the immunosuppressive TIME. In DEN-driven and CDHFD-induced MASH-HCC models, liver-specific SQLE knockin accelerated tumourigenesis, concomitant with impaired $CD8^+$ T cell effector functions (IFN-γ and Granzyme B) and induced MDSC immunosuppressive function (Arg-1). Single-cell assessment of $CD8^+$ T cells from *Sqle* tg mouse tumours further revealed that overexpression of SQLE dramatically disrupted oxidative phosphorylation and amino acid metabolism, which are associated with suppressed T cell self-renewal and effector function.[9 18 19 24] On the contrary, liver-specific *Sqle* knockout attenuated MASH-HCC by activating cytotoxic $CD8^+$ T cells and inhibition of MDSCs. Most importantly, inhibition of SQLE also augmented infiltration of human effector $CD8^+$ T cells in human MASH-HCC tumours in $CD34^+$ humanised mice. In vitro co-culture assays validated that SQLE-driven secretome impaired $CD8^+$ T cell effector functions but induced Arg-1^+ MDSC accumulation. Depletion of $CD8^+$ T cells or MSDCs abrogated the effect of SQLE manipulation on MASH-HCC in vivo, inferring that the protumourigenic function of SQLE is dependent on its impact on the TIME. Taken together, our results indicate that SQLE drives impaired immune surveillance to promote MASH-HCC.

$CD8^+$ T cells play a crucial role in antitumour immunity, but their cytotoxic function is inhibited in TIME, especially in the context of MASH.[8 9 25] Given that SQLE acts as the key rate-limiting enzyme in the cholesterol biosynthesis, we asked if excess cholesterol is causative in the immunosuppressive function of SQLE in MASH-HCC. Indeed, we found that cholesterol depletion in SQLE-overexpressing MASH-HCC cell conditioned medium abolished its inhibitory effect on $CD8^+$ T cells, whereas exogenous addition of cholesterol exerted an opposite effect in SQLE-depleted MASH-HCC cells. Consistent with our findings, others have reported that cholesterol suppresses cytotoxic T cell function by binding to T cell receptors and keeping it in an inactive conformation resistant to phosphorylation,[26] and that high cholesterol levels in TIME promote $CD8^+$ T cell exhaustion.[27] Furthermore, we revealed that SQLE and its downstream metabolite cholesterol impair $CD8^+$ T cell activity through promoting mitochondrial dysfunction. Indeed, dysfunctional mitochondria or impaired oxidative phosphorylation are known contributors of T cell exhaustion and dysfunction.[19 28 29] Taken together, our results show that SQLE-driven cholesterol accumulation diminishes the mitochondrial activity of $CD8^+$ T cells, which underlies their impaired function in SQLE-induced MASH-HCC.

MDSCs are major immunosuppressive cells in TIME of many cancers by antagonising $CD8^+$ T cell function.[30] Intriguingly, we showed that SQLE-driven immunosuppressive activity of MDSCs in MASH-HCC is also dependent on cholesterol. SQLE-induced immunosuppressive function of MDSCs, which could be reversed by cholesterol depletion using β-CD. Whereas cholesterol supplementation restored levels of Arg-1^+ MDSCs co-cultured in SQLE-knockout MASH-HCC cell conditioned medium. Previous studies suggested that lipids, such as VLDL, LDL and some types of unsaturated fatty acids, in the TIME contribute to the immunosuppressive activity of MDSCs.[31 32] Hence, the aberrant accumulation of lipids and cholesterol in MASH-HCC might contribute to an immunosuppressive TIME via MDSCs. In contrast to M2 macrophages, few studies have studied the involvement of MDSCs in MASH-HCC pathogenesis.[33] Recently, it was shown that blocking the recruitment of tumour-associated neutrophil with a CXCR2 inhibitor could potentiate the effectiveness of anti-PD-1 therapy for MASH-HCC by enhancing dendritic cell activation and $CD8^+$ T cell infiltration.[34] Hence, activation of immunosuppressive MDSCs by SQLE-mediated cholesterol accumulation further dampens effector $CD8^+$ T cells in MASH-HCC, thereby enabling immune evasion and accelerated tumourigenesis.

In contrast to virus-associated HCC,[6] recently, it has been reported that HCC with underlying MASH failed to benefit from anti-PD-1-based immunotherapy, due to the accumulation of proinflammatory and exhausted $CD8^+$ T cells.[8 9] In preclinical models, the administration of anti-PD-1 treatment even promoted fibrosis and MASH-HCC development through the reactivation of tissue-resident TNF-α^+ PD-1^+ $CD8^+$ T cells.[8 9] Hence, approaches to sensitise MASH-HCC to ICI therapies represent an unmet and urgent need. Here, we first showed SQLE as a potential immunotherapeutic target in MASH-HCC by potentiating the efficacy of ICI therapies. Using spontaneous MASH-HCC mouse models, we validated that anti-PD-1 alone was ineffective in inhibiting the progression of MASH-HCC. On the other hand, liver-specific SQLE ablation in combination anti-PD-1 restored the effectiveness of anti-PD-1 treatment in MASH-HCC. More importantly, we repurposed terbinafine, an Food and Drug Administration (FDA)-approved SQLE targeting drug for treatment of fungal infections, in combination with ICI therapies. Consistent with that of *Sqle* knockout, addition of terbinafine boosted anti-PD-1 response in spontaneous MASH-HCC in mice. Either *Sqle* knockout or terbinafine mediated tumour suppression by reactivating cytotoxic $CD8^+$ T cells in MASH-HCC. In support of our approach to harness antitumour $CD8^+$ T cells in MASH-HCC, Shalapour *et al*[35] showed that targeting of programmed cell death ligand 1 (PD-L1)- and IL-10-expressing IgA^+ cells with anti-PD-L1 could eliminate HFD-induced MASH-HCC in *MUP-uPA* mice through reactivating antitumour $CD8^+$ T cells. Nevertheless, clinical testing in humans will be required to validate the beneficial effect of terbinafine in human MASH-HCC immunotherapy.

Terbinafine, an FDA-approved antifungal agent, has shown an antitumour effect in multiple cancers.[11 36] However, its effectiveness might be limited in humans as it primarily targets fungal SQLE, with only modest potency towards human SQLE isoform. Human SQLE-specific inhibitors, such as NB-598 and Cmpd-4, were much more potent inhibitors in this regard.[37] Additional studies focusing on human SQLE-specific blockers will verify whether SQLE could be a therapeutic target for boosting immunotherapy efficacy in human HCC.

Multiple lines of evidence suggest that targeting cholesterol biosynthesis exerts an antitumour effect. Statins, prototypical inhibitors of cholesterol biosynthesis, effectively prevented MASLD-HCC development in mouse models.[5 38] In support of this, a meta-analysis of 59,073 HCC patients showed that statin users had significantly lower risk of HCC development compared with statin non-users.[39] On the other hand, RCTs involving statins in HCC patients have shown mixed results. One RCT showed that pravastatin use contributed to prolonged survival in advanced HCC.[40] However, a more recent RCT reported that pravastatin combined with sorafenib failed to improve prognosis in patients with advanced HCC as compared with sorafenib alone.[41] Nevertheless, neither of these RCTs focused on MASLD-HCC. Future RCTs with MASLD-HCC patients will be required to confirm the potential effect of statins in this subset of HCC patients.

In summary, tumour-intrinsic SQLE induces an impaired antitumour surveillance in MASH-HCC by cholesterol accumulation in the TIME, which disrupts tumour-infiltrating $CD8^+$ T cell effector function and augments immunosuppressive MDSCs. Targeting SQLE is potentially promising therapeutic strategy to

reactivate cytotoxic T cells to respond to anti-PD-1 therapy in MASH-HCC (figure 7G).

Contributors JW performed the experiments, analysed the data, and drafted the manuscript. XZ and CCW commented on the study and revised the paper. YZhang, YZhou and XK performed animal experiments. AH-KC performed histological evaluation. YP, YL, FJ and DL performed experiments. JY designed and supervised the study and revised the manuscript. JY acted as the guarantor of the study.

Funding This project was supported by National Natural Science Foundation of China (NSFC; 81972576), Research Grants Council (RGC) Theme-based Research Scheme (T12-703/19-R), RGC Research Impact Fund (R4017-18F), RGC-General Research Fund (GRF) Hong Kong (14110819, 14111621), The Kingboard Precision Oncology Program, The Chinese University of Hong Kong.

Competing interests None declared.

Patient and public involvement Patients and/or the public were not involved in the design, or conduct, or reporting, or dissemination plans of this research.

Patient consent for publication Not applicable.

Ethics approval All animal studies were approved by the Animal Experimentation Ethics Committee (AEEC) of the Chinese University of Hong Kong (CUHK).

Provenance and peer review Not commissioned; externally peer reviewed.

Data availability statement All data relevant to the study are included in the article or uploaded as online supplemental information. All data supporting the findings of this study are available within the article and its online supplemental information.

ORCID iDs
Jun Wen http://orcid.org/0000-0002-6947-2087
Xiang Zhang http://orcid.org/0000-0002-3222-5824
Jun Yu http://orcid.org/0000-0001-5008-2153

REFERENCES

1 Younossi ZM, Koenig AB, Abdelatif D, *et al*. Global epidemiology of Nonalcoholic fatty liver disease-meta-analytic assessment of prevalence, incidence, and outcomes. *Hepatology* 2016;64:73–84.
2 Estes C, Anstee QM, Arias-Loste MT, *et al*. Modeling NAFLD disease burden in China, France, Germany, Italy, Japan, Spain, United kingdom, and United States for the period 2016-2030. *J Hepatol* 2018;69:896–904.
3 Huang DQ, El-Serag HB, Loomba R. Global epidemiology of NAFLD-related HCC: trends, predictions, risk factors and prevention. *Nat Rev Gastroenterol Hepatol* 2021;18:223–38.
4 Foerster F, Gairing SJ, Müller L, *et al*. NAFLD-driven HCC: safety and efficacy of current and emerging treatment options. *J Hepatol* 2022;76:446–57.
5 Zhang X, Coker OO, Chu ES, *et al*. Dietary cholesterol drives fatty liver-associated liver cancer by Modulating gut Microbiota and metabolites. *Gut* 2021;70:761–74.
6 Sangro B, Sarobe P, Hervás-Stubbs S, *et al*. Advances in Immunotherapy for hepatocellular carcinoma. *Nat Rev Gastroenterol Hepatol* 2021;18:525–43.
7 Wang Z, Aguilar EG, Luna JI, *et al*. Paradoxical effects of obesity on T cell function during tumor progression and PD-1 Checkpoint blockade. *Nat Med* 2019;25:141–51.
8 Pfister D, Núñez NG, Pinyol R, *et al*. NASH limits anti-tumour surveillance in Immunotherapy-treated HCC. *Nature* 2021;592:450–6.
9 Wabitsch S, McCallen JD, Kamenyeva O, *et al*. Metformin treatment Rescues Cd8(+) T-cell response to immune Checkpoint inhibitor therapy in mice with NAFLD. *J Hepatol* 2022;77:748–60.
10 Meyer T, Galani S, Lopes A, *et al*. Aetiology of liver disease and response to immune Checkpoint inhibitors: an updated meta-analysis CONFIRMS benefit in those with non-viral liver disease. *J Hepatol* 2023;79:e73–6.
11 Liu D, Wong CC, Fu L, *et al*. Squalene Epoxidase drives NAFLD-induced hepatocellular carcinoma and is a pharmaceutical target. *Sci Transl Med* 2018;10:eaap9840.
12 Liu D, Wong CC, Zhou Y, *et al*. Squalene Epoxidase induces Nonalcoholic Steatohepatitis via binding to carbonic Anhydrase III and is a therapeutic target. *Gastroenterology* 2021;160:2467–82.
13 Kishida N, Matsuda S, Itano O, *et al*. Development of a novel mouse model of hepatocellular carcinoma with Nonalcoholic Steatohepatitis using a high-fat, choline-deficient diet and intraperitoneal injection of diethylnitrosamine. *BMC Gastroenterol* 2016;16:61.
14 Zhao R, Coker OO, Wu J, *et al*. Aspirin reduces colorectal tumor development in mice and gut Microbes reduce its Bioavailability and chemopreventive effects. *Gastroenterology* 2020;159:969–83.
15 Dudek M, Pfister D, Donakonda S, *et al*. Auto-aggressive Cxcr6(+) Cd8 T cells cause liver immune pathology in NASH. *Nature* 2021;592:444–9.
16 Bao Y, Zhai J, Chen H, *et al*. Targeting M(6)A reader Ythdf1 augments Antitumour immunity and BOOSTS anti-PD-1 efficacy in colorectal cancer. *Gut* 2023;72:1497–509.
17 Wu M-J, Shi L, Dubrot J, *et al*. Mutant IDH inhibits IFNγ-Tet2 signaling to promote Immunoevasion and tumor maintenance in Cholangiocarcinoma. *Cancer Discov* 2022;12:812–35.
18 Ringel AE, Drijvers JM, Baker GJ, *et al*. Obesity shapes metabolism in the tumor Microenvironment to suppress anti-tumor immunity. *Cell* 2020;183:1848–66.
19 Vardhana SA, Hwee MA, Berisa M, *et al*. Impaired mitochondrial oxidative Phosphorylation limits the self-renewal of T cells exposed to persistent antigen. *Nat Immunol* 2020;21:1022–33.
20 Choi Y, Lee S, Kim K, *et al*. Studying cancer Immunotherapy using patient-derived Xenografts (Pdxs) in Humanized mice. *Exp Mol Med* 2018;50:1–9.
21 Wong CC, Wu J-L, Ji F, *et al*. The cholesterol uptake regulator Pcsk9 promotes and is a therapeutic target in APC/KRAS-mutant colorectal cancer. *Nat Commun* 2022;13:3971.
22 Mahammad S, Parmryd I. Cholesterol depletion using methyl-**B**-Cyclodextrin. In: Owen DM, ed. *Methods in Membrane Lipids*. New York, NY: Springer New York, 2015: 91–102.
23 Thomas DA, Massagué J. TGF-beta directly targets cytotoxic T cell functions during tumor evasion of immune surveillance. *Cancer Cell* 2005;8:369–80.
24 Geiger R, Rieckmann JC, Wolf T, *et al*. L-arginine modulates T cell metabolism and enhances survival and anti-tumor activity. *Cell* 2016;167:829–42.
25 Wolf MJ, Adili A, Piotrowitz K, *et al*. Metabolic activation of Intrahepatic Cd8+ T cells and NKT cells causes Nonalcoholic Steatohepatitis and liver cancer via cross-talk with hepatocytes. *Cancer Cell* 2014;26:549–64.
26 Swamy M, Beck-Garcia K, Beck-Garcia E, *et al*. A cholesterol-based Allostery model of T cell receptor Phosphorylation. *Immunity* 2016;44:1091–101.
27 Ma X, Bi E, Lu Y, *et al*. Cholesterol induces Cd8(+) T cell exhaustion in the tumor Microenvironment. *Cell Metab* 2019;30:143–56.
28 Yu Y-R, Imrichova H, Wang H, *et al*. Disturbed mitochondrial Dynamics in Cd8(+) Tils reinforce T cell exhaustion. *Nat Immunol* 2020;21:1540–51.
29 Scharping NE, Menk AV, Moreci RS, *et al*. The tumor Microenvironment represses T cell mitochondrial Biogenesis to drive Intratumoral T cell metabolic insufficiency and dysfunction. *Immunity* 2016;45:374–88.
30 Veglia F, Perego M, Gabrilovich D. Myeloid-derived Suppressor cells coming of age. *Nat Immunol* 2018;19:108–19.
31 Al-Khami AA, Zheng L, Del Valle L, *et al*. Exogenous lipid uptake induces metabolic and functional Reprogramming of tumor-associated myeloid-derived Suppressor cells. *Oncoimmunology* 2017;6:e1344804.
32 Yan D, Adeshakin AO, Xu M, *et al*. Lipid metabolic pathways confer the immunosuppressive function of myeloid-derived Suppressor cells in tumor. *Front Immunol* 2019;10:1399.
33 Ambade A, Satishchandran A, Saha B, *et al*. Hepatocellular carcinoma is accelerated by NASH involving M2 macrophage polarization mediated by Hif-1Ainduced IL-10. *Oncoimmunology* 2016;5:e1221557.
34 Leslie J, Mackey JBG, Jamieson T, *et al*. Cxcr2 inhibition enables NASH-HCC Immunotherapy. *Gut* 2022;71:2093–106.
35 Shalapour S, Lin X-J, Bastian IN, *et al*. Inflammation-induced Iga+ cells dismantle anti-liver cancer immunity. *Nature* 2017;551:340–5.
36 Brown DN, Caffa I, Cirmena G, *et al*. Squalene Epoxidase is a BONA fide Oncogene by amplification with clinical relevance in breast cancer. *Sci Rep* 2016;6:19435.
37 Padyana AK, Gross S, Jin L, *et al*. Structure and inhibition mechanism of the catalytic domain of human Squalene Epoxidase. *Nat Commun* 2019;10:97.
38 Pan Y, Chen H, Zhang X, *et al*. Mettl3 drives NAFLD-related hepatocellular carcinoma and is a therapeutic target for boosting Immunotherapy. *Cell Rep Med* 2023;4:101144.
39 Islam MdM, Poly TN, Walther BA, *et al*. n.d. Statin use and the risk of hepatocellular carcinoma: A meta-analysis of observational studies. *Cancers*12:671.
40 Kawata S, Yamasaki E, Nagase T, *et al*. Effect of pravastatin on survival in patients with advanced hepatocellular carcinoma. A randomized controlled trial. *Br J Cancer* 2001;84:886–91.
41 Jouve J-L, Lecomte T, Bouché O, *et al*. Pravastatin combination with sorafenib does not improve survival in advanced hepatocellular carcinoma. *J Hepatol* 2019;71:516–22.

Fig. S1

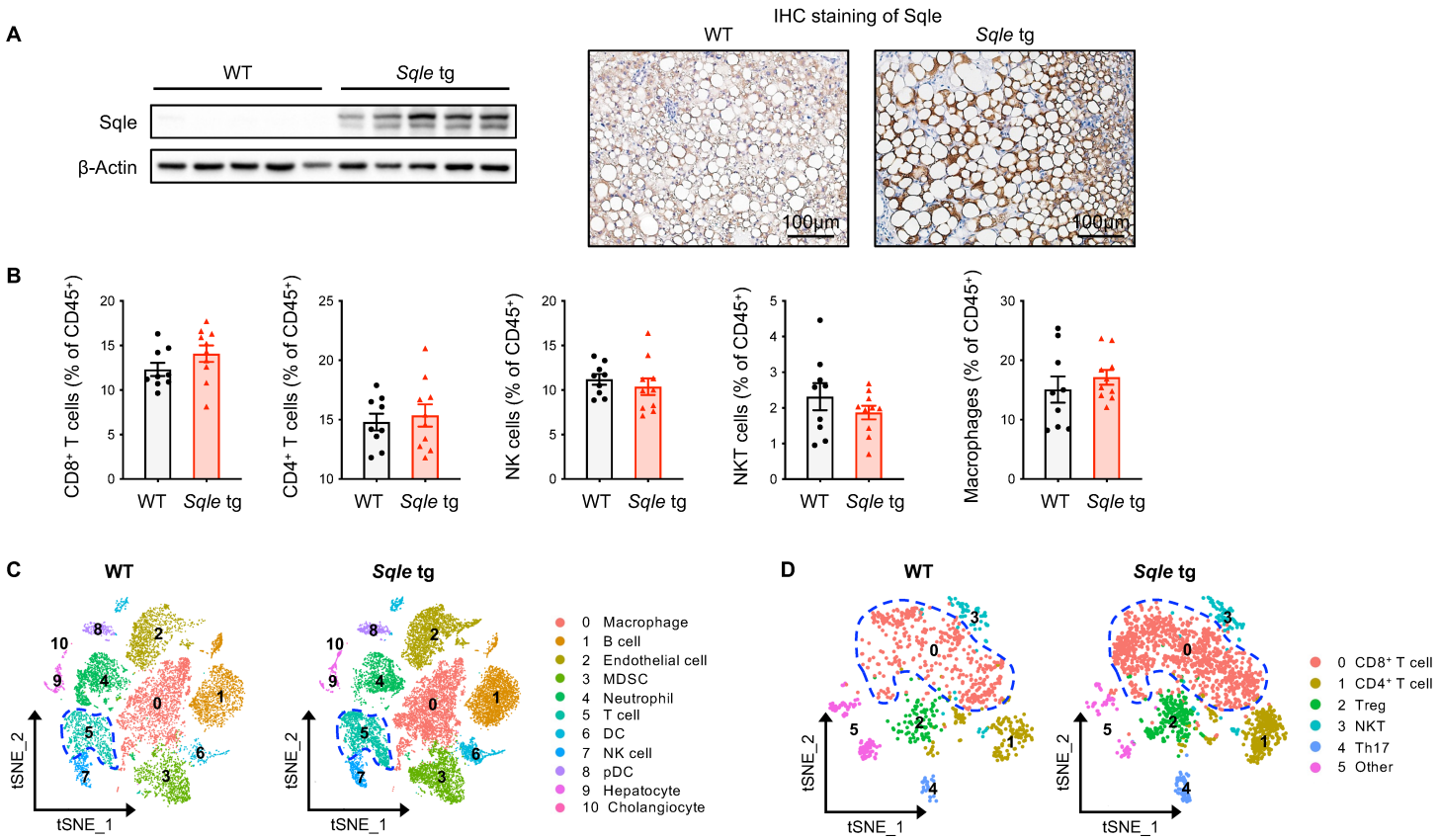

Cluster	Cell type	Key differentially expressed transcripts
0	Macrophage	Itgam, Adgre1, C1qc, Mrc1, Cd5l
1	B cell	Cd79a, Cd79b, Ighm, Iglc2, Cd19
2	Endothelial cell	Sparc, Pecam1, Fabp4, Tek, Lyve1
3	MDSC	Itgam, Il1b, Fn1, Il1rn, Prdx1
4	Neutrophil	Itgam, S100a8, Retnlg, Hp, Msrb1
5	T cell	Cd3e, Cd3d, Trbc1, Thy1
6	DC	H2-Aa, Syngr2, Cd83, Cd74, Flt3, Batf3
7	NK cell	Ncr1, Klra7, Klre1
8	pDC	Siglech, Bst2, Ccr9
9	Hepatocyte	Alb, Serpina3k, Apoa1
10	Cholangiocyte	Epcam, Krt7, Krt19, Clu

Cluster	Cell type	Key differentially expressed transcripts
0	CD8⁺ T cell	Cd8a, Cd3e, Trbc1
1	CD4⁺ T cell	Cd4, Cd3e, Trbc1
2	Treg	Cd4, Foxp3, Ikzf2, Ccr8
3	NKT	Ncr1, Klra7, Klre1, Cd3e, Trbc1
4	Th17	Il17a, Il23r, Rorc, Furin
5	Other	Cd3e, Trbc1 (without high expression of neither Cd4 nor Cd8a)

Fig. S1. (**A**) Overexpression of Sqle in the livers of *Sqle tg* mice was confirmed by western blot (*Left*) and immunohistochemistry (IHC) staining (*Right*). (**B**) Percentages of intratumoral CD8$^+$ T cells, CD4$^+$ T cells, NK cells, NKT cells, and macrophages in WT and *Sqle* tg mice determined by flow cytometry. (**C**) tSNE plots of CD45$^+$ cells derived from tumors of WT or *Sqle* tg mice (*Upper*). Tumors isolated from three different mice of the same group were pooled per sample, and two samples per group were prepared for subsequent sequencing (n=2 per group). Two samples from the same group were presented in one tSNE plot. Each dot represents a single cell. Key differentially expressed transcripts that define each cell cluster are shown (*Down*). (**D**) tSNE plots of T lymphocytes (cluster #5 in fig. S1C) derived from tumors of WT or *Sqle* tg mice (*Upper*). Two samples from the same group were presented in one tSNE plot. Key differentially expressed transcripts that define each cell sub-cluster are shown (*Down*).

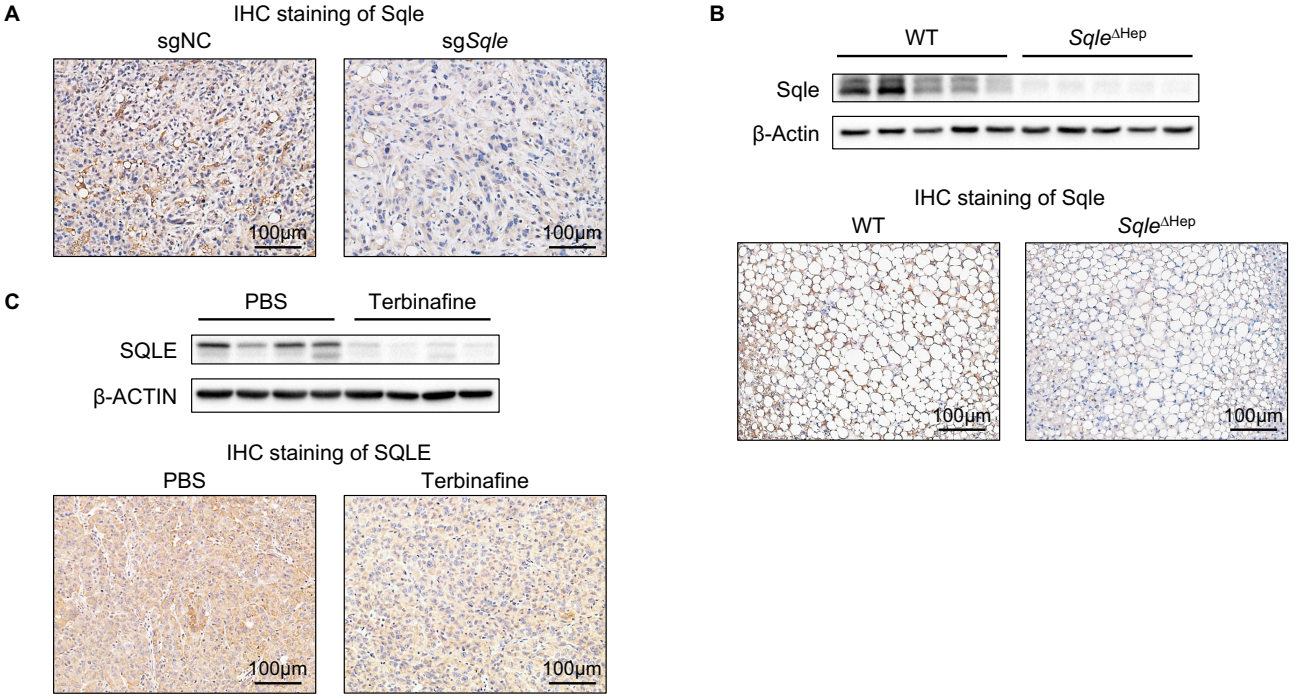

Fig. S2. (**A**) Knockout of Sqle in RIL-175 orthotopic tumors was confirmed by IHC staining. (**B**) Knockout of Sqle in the livers of *Sqle*$^{\Delta Hep}$ mice was confirmed by western blot (*Upper*) and IHC staining (*Down*). (**C**) Inhibition of terbinafine on SQLE of HKCI2 subcutaneous tumors in humanized mice was confirmed by western blot (*Upper*) and IHC staining (*Down*).

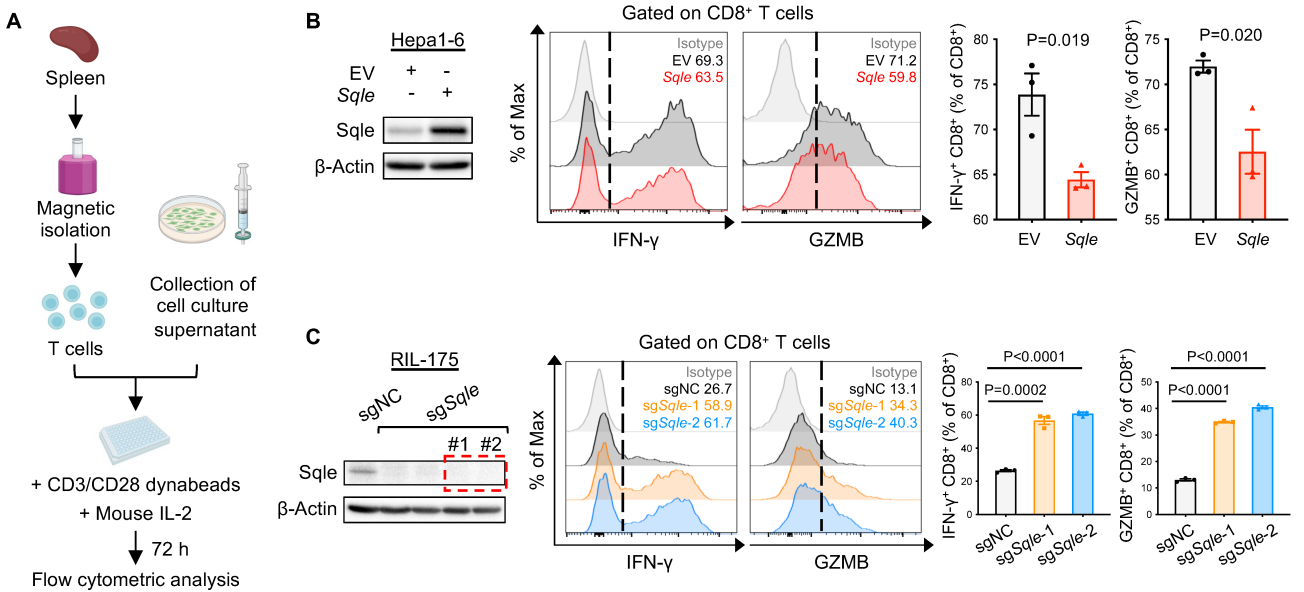

Fig. S3. (**A**) T cells harvested from tumor-free mouse spleens were treated with indicated conditioned medium for 72 h and were collected to be analyzed by flow cytometry. (**B**) Flow cytometry of IFN-γ$^+$ or Granzyme B$^+$ CD8$^+$ T cells treated with conditioned medium of Hepa1-6 cells with or without overexpression of SQLE. (**C**) Flow cytometry of IFN-γ$^+$ or Granzyme B$^+$ CD8$^+$ T cells treated with conditioned medium of RIL-175 cells with or without SQLE knockout.

Fig. S4

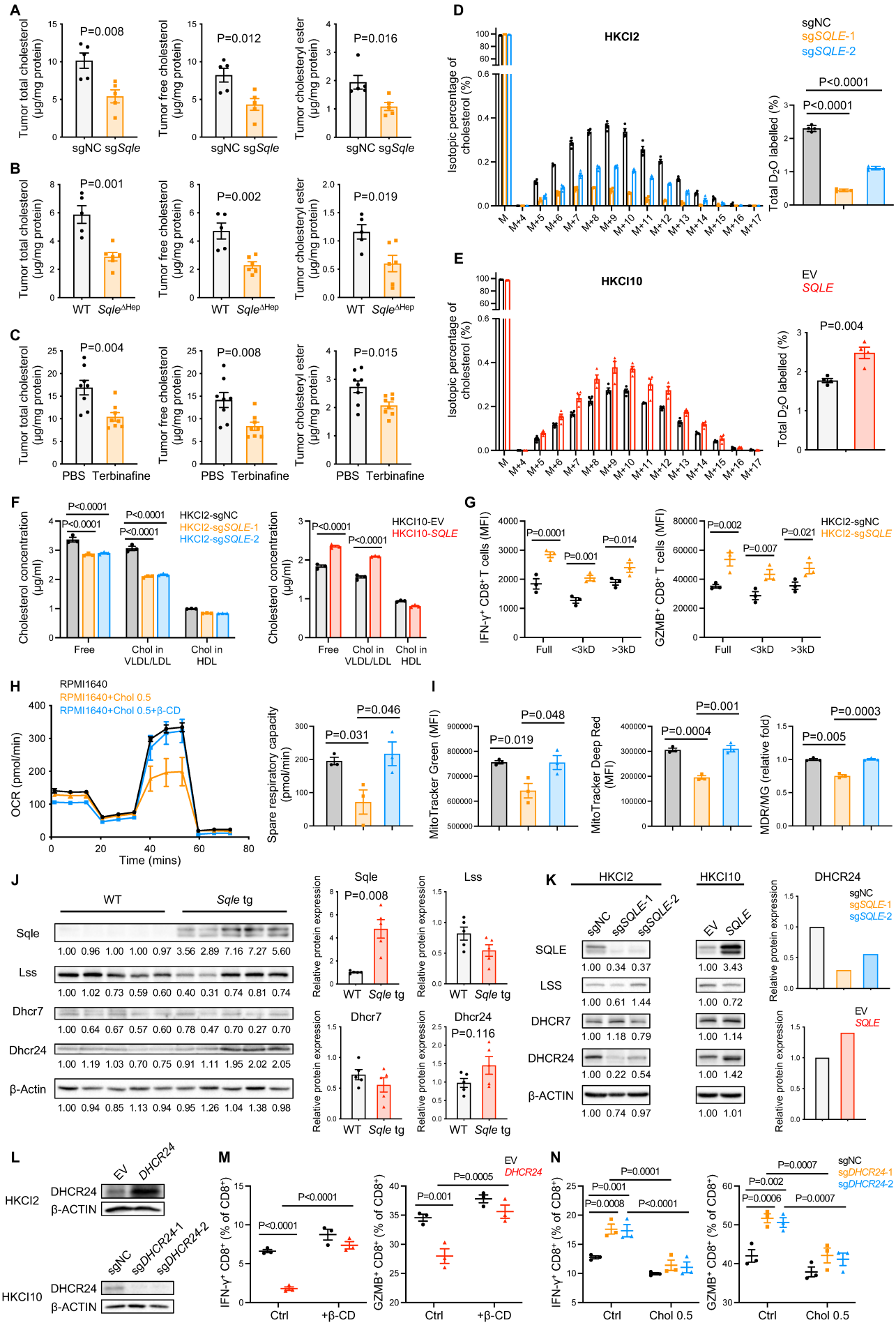
A
Tumor total cholesterol (μg/mg protein)
P=0.008
Tumor free cholesterol (μg/mg protein)
P=0.012
Tumor cholesteryl ester (μg/mg protein)
P=0.016
sgNC sgSqle
B
P=0.001
P=0.002
P=0.019
WT SqleΔHep
C
P=0.004
P=0.008
P=0.015
PBS Terbinafine
D
HKCI2
Isotopic percentage of cholesterol (%)
M M+4 M+5 M+6 M+7 M+8 M+9 M+10 M+11 M+12 M+13 M+14 M+15 M+16 M+17
sgNC
sgSQLE-1
sgSQLE-2
P<0.0001
P<0.0001
Total D2O labelled (%)
E
HKCI10
EV
SQLE
P=0.004
F
Cholesterol concentration (μg/ml)
HKCI2-sgNC
HKCI2-sgSQLE-1
HKCI2-sgSQLE-2
Free
Chol in VLDL/LDL
Chol in HDL
HKCI10-EV
HKCI10-SQLE
G
IFN-γ+ CD8+ T cells (MFI)
P=0.0001
P=0.001
P=0.014
Full
<3kD
>3kD
GZMB+ CD8+ T cells (MFI)
P=0.002
P=0.007
P=0.021
HKCI2-sgNC
HKCI2-sgSQLE
H
RPMI1640
RPMI1640+Chol 0.5
RPMI1640+Chol 0.5+β-CD
OCR (pmol/min)
Time (mins)
Spare respiratory capacity (pmol/min)
P=0.031
P=0.046
I
MitoTracker Green (MFI)
P=0.019
P=0.048
MitoTracker Deep Red (MFI)
P=0.0004
P=0.001
MDR/MG (relative fold)
P=0.005
P=0.0003
J
WT
Sqle tg
Sqle
1.00 0.96 1.00 1.00 0.97 3.56 2.89 7.16 7.27 5.60
Lss
1.00 1.02 0.73 0.59 0.60 0.40 0.31 0.74 0.81 0.74
Dhcr7
1.00 0.64 0.67 0.57 0.60 0.78 0.47 0.70 0.27 0.70
Dhcr24
1.00 1.19 1.03 0.70 0.75 0.91 1.11 1.95 2.02 2.05
β-Actin
1.00 0.94 0.85 1.13 0.94 0.95 1.26 1.04 1.38 0.98
Relative protein expression
P=0.008
P=0.116
K
HKCI2
HKCI10
sgNC
sgSQLE-1
sgSQLE-2
EV
SQLE
SQLE
1.00 0.34 0.37
1.00 3.43
LSS
1.00 0.61 1.44
1.00 0.72
DHCR7
1.00 1.18 0.79
1.00 1.14
DHCR24
1.00 0.22 0.54
1.00 1.42
β-ACTIN
1.00 0.74 0.97
1.00 1.01
DHCR24
sgNC
sgSQLE-1
sgSQLE-2
EV
SQLE
L
HKCI2
DHCR24
β-ACTIN
EV
DHCR24
HKCI10
sgNC
sgDHCR24-1
sgDHCR24-2
M
IFN-γ+ CD8+ (% of CD8+)
P<0.0001
P<0.0001
Ctrl
+β-CD
GZMB+ CD8+ (% of CD8+)
P=0.001
P=0.0005
EV
DHCR24
N
IFN-γ+ CD8+ (% of CD8+)
P=0.0001
P=0.001
P=0.0008
P<0.0001
Ctrl
Chol 0.5
GZMB+ CD8+ (% of CD8+)
P=0.0007
P=0.002
P=0.0006
P=0.0007
sgNC
sgDHCR24-1
sgDHCR24-2

Fig. S4

Fig. S4. (**A**) Total and free cholesterol concentrations in the tumors of orthotopic RIL-175 mouse model. (**B**) Total and free cholesterol concentrations in the tumors of DEN-injected CDHFD-fed MASH-HCC WT and hepatocyte-specific *Sqle* knockout mice. (**C**) Total and free cholesterol concentrations in HKCI2 subcutaneous tumors of humanized mouse model. (**D** and **E**) D_2O stable isotope labelling (48 h) of *de novo* synthesized cholesterol and LC-MS analysis of deuterium incorporated into cholesterol in HKCI2 (**D**) and HKCI10 (**E**) isogenic cells. (**F**) The conditioned medium of HKCI2 or HKCI10 cells was separated into low (<3kDa) and high (>3kDa) molecular weight fractions. Concentrations of free cholesterol and lipoprotein cholesterol were quantified separately. (**G**) The low (<3kDa) and high (>3kDa) molecular weight fractions of HKCI2-sgNC or -sg*SQLE* conditioned medium were used to culture T cells. $CD8^+$ T cell function was analyzed by flow cytometry. (**H**) Oxygen consumption rate (OCR) and spare respiratory capacity (SRC) were measured using seahorse analysis on $CD8^+$ T cells treated with RPMI1640 medium with or without the addition of cholesterol (0.5 μg/ml) and β-CD (0.5mM). (**I**) MFI of MitoTracker Green (MG) and MitoTracker Deep Red (MDR), and the ratio of MDR to MG of $CD8^+$ T cells treated with RPMI1640 medium with or without the addition of cholesterol (0.5 μg/ml) and β-CD (0.5mM). (**J** and **K**) Protein expression levels of SQLE downstream enzymes in cholesterol biosynthesis, namely LSS, DHCR7, and DHCR24, in *Sqle* tg mice (**J**), SQLE-knockout HKCI2 cells, and SQLE-overexpressing HKCI10 cells (**K**) were determined by western blot. (**L**) DHCR24 overexpression in HKCI2 cells and DHCR24 knockout in HKCI10 cells were validated by western blot. (**M**) Flow cytometric analysis of IFN-γ^+ or Granzyme B^+ $CD8^+$ T cells treated with the conditioned medium of HCKI2 cells with or without the overexpression of DHCR24, with or without β-CD (0.5mM). (**N**) Flow cytometric analysis of IFN-γ^+ or Granzyme B^+ $CD8^+$ T cells treated with the conditioned medium of HCKI10 cells with or without DHCR24 knockout, with or without the addition of cholesterol (0.5 μg/ml).

Fig. S5

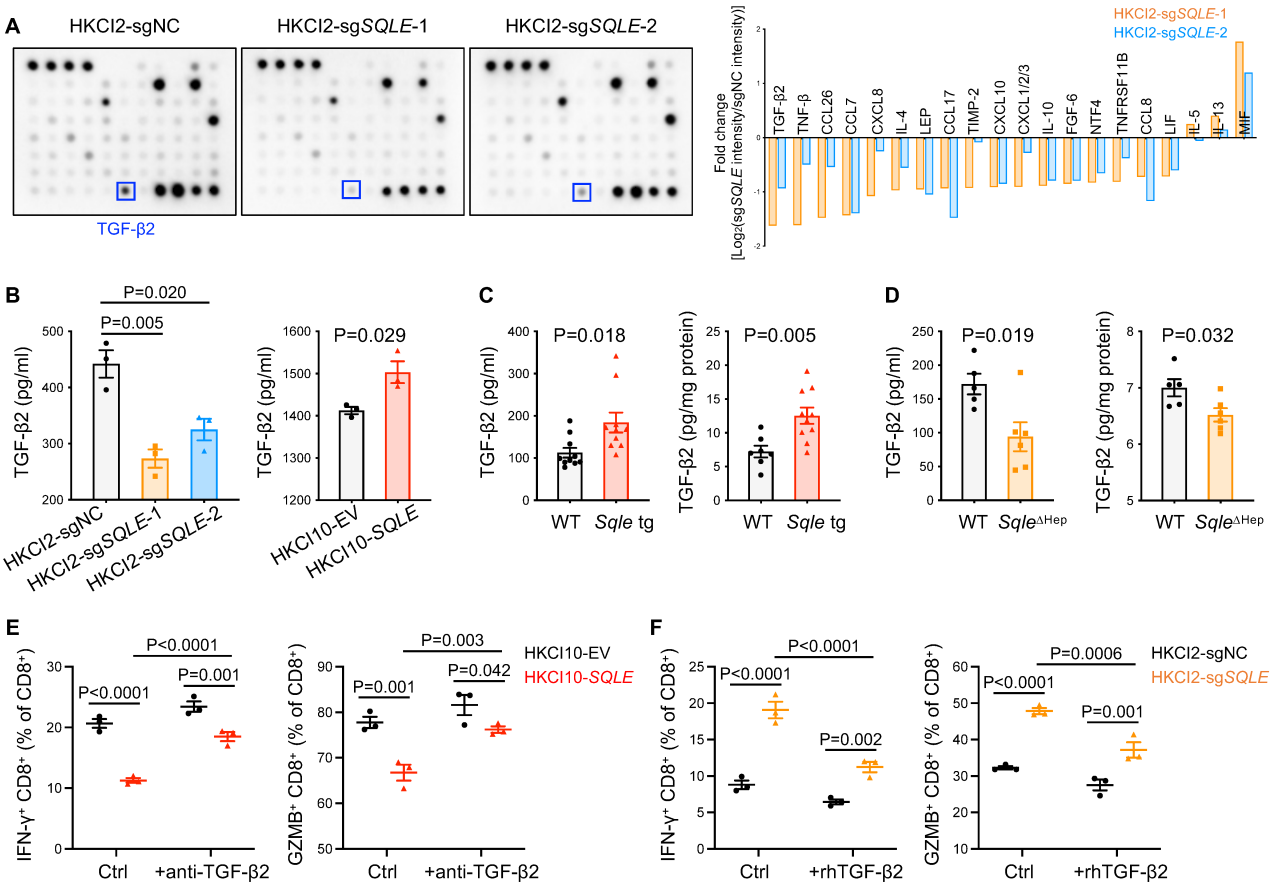

Fig. S5. (**A**) Cytokine antibody array was conducted on the conditioned medium of HKCI2 cells with or without SQLE knockout (*Left*). Densitometry showed TGF-β2 was the top down-regulated cytokine (*Right*). (**B**) ELISA measured TGF-β2 levels in the conditioned medium of SQLE-knockout and –overexpressing cells. (**C** and **D**) ELISA measured TGF-β2 levels in the serum and tumor lysates of hepatocyte-specific *Sqle* tg (**C**) and *Sqle* knockout (**D**) mice. (**E**) T cells were treated with the conditioned medium of HKCI10 cells with or without SQLE overexpression, with or without the addition of anti-TGF-β2 antibody (1 μg/ml), then measured by flow cytometry. (**F**) T cells were treated with the conditioned medium of HKCI2 cells with or without SQLE knockout, with or without the supplement of recombinant human TGF-β2 (10 ng/ml), then measured by flow cytometry.

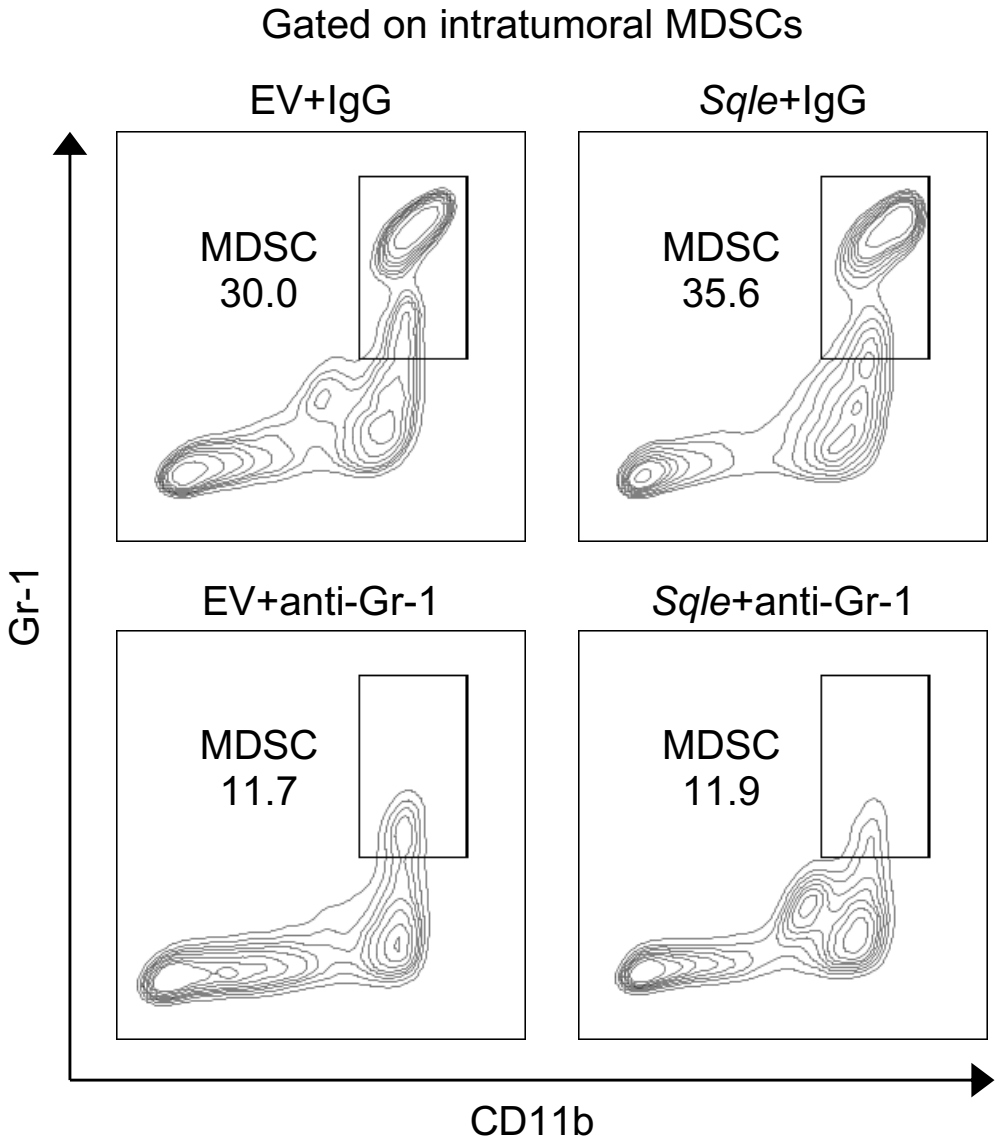

Fig. S6. Representative flow cytometric plots showed depletion efficiency of MDSCs in orthotopic tumors.

Fig. S7

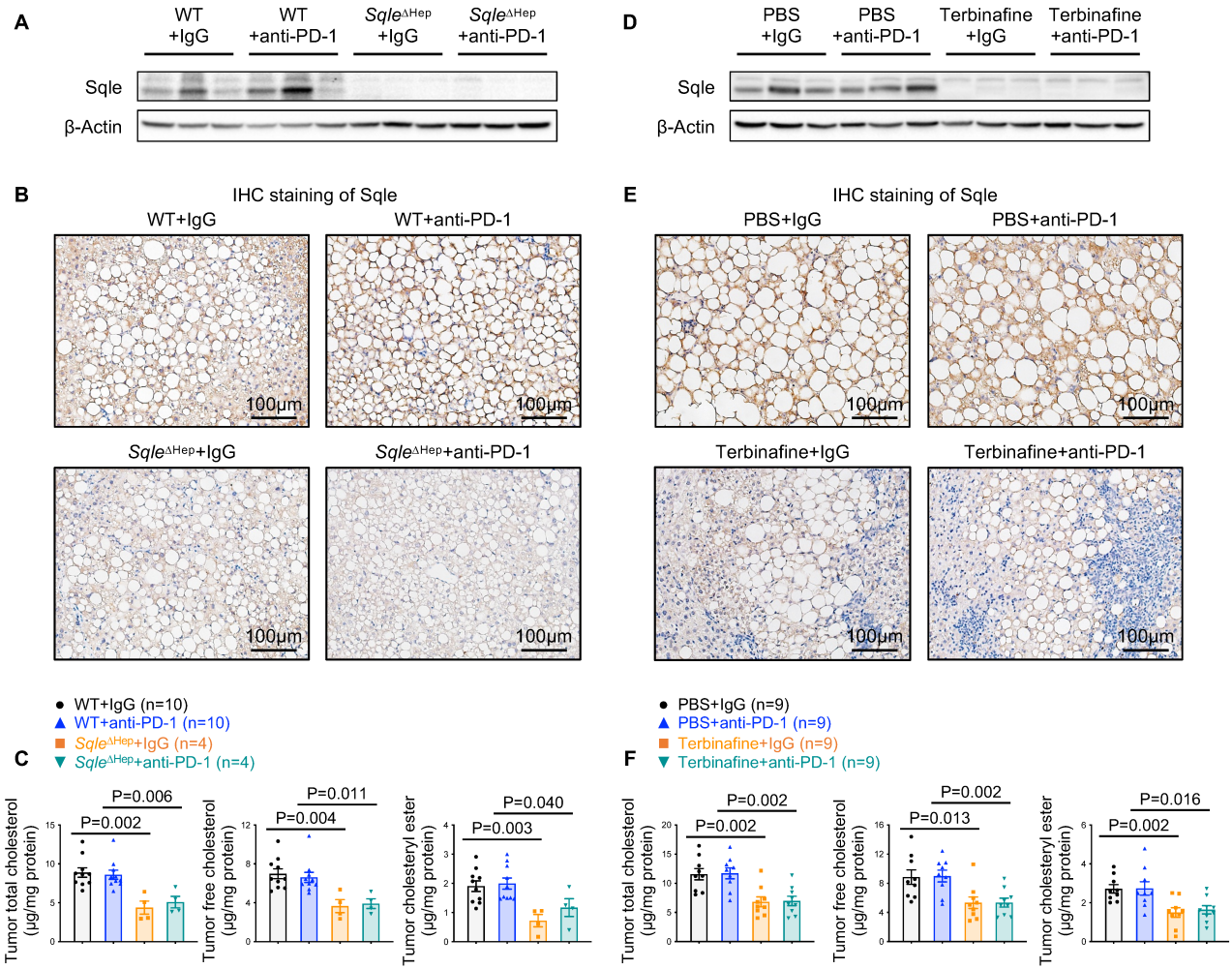

Fig. S7. (**A** and **B**) Knockout of Sqle in the livers of *Sqle*$^{\Delta Hep}$ mice in Fig. 7A was confirmed by western blot (**A**) and IHC staining (**B**). (**C**) Total cholesterol and free cholesterol concentrations in the tumors of mice in Fig. 7A were quantified. (**D** and **E**) Inhibition of terbinafine on Sqle in DEN-injected CDHFD-induced MASH-HCC mouse model in Fig. 7D was confirmed by western blot (**D**) and IHC staining (**E**). (**F**) Total cholesterol and free cholesterol concentrations in the tumors of mice in Fig. 7D were quantified.

Fig. S8

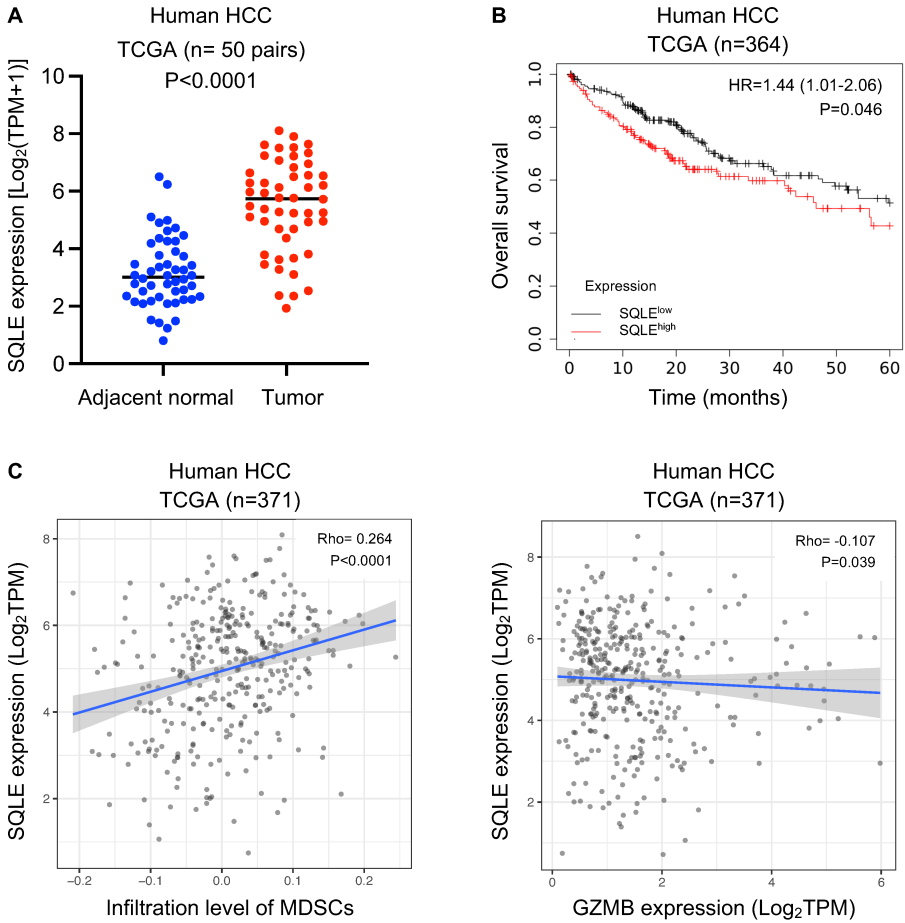

Fig. S8. (**A**) Expression of SQLE in human HCC and paired adjacent normal tissues was determined in TCGA cohort. (**B**) High SQLE expression was associated with poor survival in human HCC in TCGA cohort. (**C**) The association between SQLE expression and MDSC infiltration (*left*) or GZMB expression (*right*) was analyzed using TIMER2.0.

Supplementary Methods

Single-cell RNA sequencing

Fresh tumors isolated from WT or *Sqle* tg mouse of DEN-injected CDHFD-fed MASH-HCC were minced, washed with PBS, and digested twice in RPMI 1640 medium containing enzyme mixture of 0.35% collagenase IV, 120 U/ml DNase I, and 2 mg/ml papain for 15 mins at 37 °C with gentle rotation. Cell suspension was filtered through a 70 μm cell strainer, and tumor-infiltrating $CD45^+$ cells were enriched using CD45 (TIL) microbeads (Miltenyi Biotec). Tumors isolated from three different mice of the same group were pooled per sample, and two samples per group were prepared for library generation (10X Genomics Chromium Next GEM Single Cell 5' Kit) and sequenced on the Illumina NovaSeq 6000 system (double-end sequencing, 150bp).

scRNA-seq analyses

Libraries were sequenced at a mean sequencing depth ranging from 45,000 to 120,000 reads per cell. The scRNA-seq sequencing data were converted to FASTQ format using bcl2fastq software (v5.0.1). The sequencing data were compared to reference genome using Cell Ranger software (v7.0.0), and individual cellular 5' end transcripts were identified and counted. The expression profile matrix output by Cell Ranger was loaded into R (4.1.2) using Seurat (v4.1.0) for subsequent filtering of low-quality cells, normalization, dimensional reduction, and clustering. Single-cell transcripts were filtered according to the following criteria: (1) cells in which fewer than 500 genes were detected, or (2) cells with the proportion of mitochondrial transcripts > 25%, or (3) multiple cells in one GEM.

After filtration, the expression matrix contained 29,920 cells, with 11,011 cells from WT tumors and 18,909 cells from *Sqle* tg tumors. All downstream analyses were based on the

filtered high-quality cells. Dimensional reduction was accomplished by calculating gene expression values using the LogNormalize method, followed by performing principal component analysis (PCA) based on the normalized expression values using the top 20 principal components for clustering, and subsequently, visualized by t-Distributed Stochastic Neighbor Embedding (t-SNE). Major cell types were identified based on the expression of a set of indicative markers (figure S1C and S1D).

To assess differential enrichment of Kyoto Encyclopedia of Genes and Genomes (KEGG) metabolic pathways between $CD8^+$ T cells derived from *Sqle* tg and WT mouse tumors, gene set variation analysis (GSVA), a non-parametric unsupervised analysis method, was utilized. The result of GSVA was visualized using a bar plot.

Flow cytometric analysis

Tumors, liver tissues, and peripheral blood mononuclear cells (PBMCs) were harvested. After mechanical dissection, tumors and liver tissues were digested with Collagenase IV (Sigma-Aldrich) and DNase I (Sigma-Aldrich) at 37 °C for 30 mins with gentle rotation, followed by filtration through 70 μm strainers. Cells were collected, washed with PBS, and incubated with anti-CD16/32 antibody (Biolegend) to block Fc receptors for 10 mins at 4 °C, followed by immunostaining. For stimulation, cells were incubated at 37 °C under 5% CO_2 for 3 h, with a 1:500 cell stimulation cocktail (eBioscience). For intracellular staining, samples were fixed using Foxp3/transcription factor fixation/permeabilization set (eBioscience). Surface and intracellular staining were performed using antibodies listed in table S1. Samples were analyzed by FACSVerse or FACSCelesta (BD Biosciences), and the data were analyzed using FlowJo software (v10.8.1).

Assessment of human T cell effector function

PBMCs were freshly isolated from buffy coats of healthy donors using Ficoll-Paque Premium (Cytiva). Naïve T cells were isolated from PBMCs using human T cell isolation kit (STEMCELL) and cultured in cell culture supernatants in the presence of human T-activator CD3/CD28 dynabeads (Invitrogen) and recombinant human IL-2 (10 ng/ml, Biolegend). After 72 h co-culture, dynabeads were removed and cells were collected for further phenotypic and functional analysis using flow cytometry.

Mitochondrial function assays

Human peripheral blood $CD8^+$ T cells (STEMCELL) were cultured in the indicated conditioned medium for 48 h at 37 °C. Cells were then collected for MitoTracker Green and Mitotracker Deep Red (Invitrogen) staining to measure mitochondrial mass and membrane potential.

Seahorse culture plates were treated with 25 µl/well of 22.4 µg/ml of Cell-Tak (Corning) for 20 mins at RT. Cell-Tak solution was then removed and plates was washed twice with 200 µl sterile MilliQ water/well, air dried, and kept at 4 °C until the assay was conducted. Human peripheral blood $CD8^+$ T cells (STEMCELL) were cultured in the indicated conditioned medium for 48 h at 37 °C. Cells were then collected and seeded on Cell-Tak-coated plates (1×10^5 $CD8^+$ T cells per well) in Seahorse XF RPMI Medium supplemented with 1 mM pyruvate, 2 mM glutamine, and 10 mM glucose. Cells were centrifuged at 300 g for 2 mins, and incubated for 45 mins at 37 °C. Cells were monitored in basal respiration condition and stimulated with oligomycin (1.5 µM), FCCP (1 µM), and rotenone/antimycin A (0.5 µM) using Seahorse XFe96 Analyzer (Agilent). Spare respiratory capacity (SRC) was calculated as

the difference between the mean of initial oxygen consumption rate (OCR) values and the maximal OCR values achieved after FCCP added.

Evaluation of MDSC function and T cell suppression assay

Orthotopic tumors were freshly isolated from mice and immune cells were enriched by Percoll. Mouse spleen was minced, filtered through a 70 μm cell strainer, and then resuspended with 2 ml RBC lysis buffer on ice for 5 mins. The cell suspension derived from mouse tumor or spleen was purified for MDSCs using mouse MDSC ($CD11b^+Gr1^+$) isolation kit (STEMCELL). The isolated MDSCs from tumors were divided into three parts for RNA extraction, flow cytometry, and co-culture assays. Freshly isolated T cells from mouse spleen using mouse T cell isolation kit (STEMCELL) were labelled with or without carboxyfluorescein succinimidyl ester (CFSE; Invitrogen) and co-cultured with MDSCs (MDSC: T ratio=1:1 or 1:2) in the presence of mouse CD3/CD28 dynabeads (Invitrogen) and mouse IL-2 (10 ng/ml, Biolegend) for 72 h. After 72 h of co-culture, dynabeads were removed, and cells were collected for intracellular staining of IFN-γ and Granzyme B. CFSE signal intensity and functional marker intensity were acquired by flow cytometry. Human MDSCs were induced from PBMCs of healthy donors by adding recombinant human granulocyte-macrophage colony-stimulating factor (GM-CSF) (Biolegend) and IL-6 (Biolegend) (20 ng/ml) in RPMI1640 medium at 37 °C in a humidified incubator containing 5% CO_2 for 5 days. Yield and purity of MDSCs were confirmed by flow cytometry.

Cell lines and cell culture

Two human MASH-HCC cell lines HKCI2 and HKCI10 were generated previously from MASH-HCC patients by Prof. Nathalie Wong (Department of Surgery, CUHK)[1]. Murine HCC cell line RIL-175 was kindly provided by Dr. Greten and Prof. Zender[2]. The above cells were cultured in RPMI 1640 medium (Gibco, Thermo Fisher Scientific) supplemented with 10%

fetal bovine serum (Gibco) and maintained at 37 °C in a humidified incubator containing 5% CO_2.

Murine Hepa1-6 cells were purchased from purchased from the American Type Culture Collection (ATCC). The 293T cell line was purchased from Invitrogen (Thermo Fisher Scientific). The above two types of cell line were cultured in Dulbecco's Modified Eagle Medium (Gibco, Thermo Fisher Scientific) supplemented with 10% fetal bovine serum (Gibco) and maintained at 37 °C in a humidified incubator containing 5% CO_2.

Construction of organoids derived from primary mouse liver tumors

Tumors derived from WT or *Sqle* tg mice were freshly collected and washed with PBS. Tumors were cut into small pieces, washed with PBS for three times to remove grease in the supernatant, minced into smaller pieces with the addition of digestion medium, and then incubated at 37 °C under 5% CO_2 for 2 h, with gentle shaking every 20 mins. The cell suspension was filtered through a 70 μm cell strainer, and then resuspended with 2 ml RBC lysis buffer (Biolegend) on ice for 5 mins. After centrifugation, the cell pellet was resuspended in appropriate volume of mouse liver organoid medium mixed with appropriate volume of Matrigel (Corning), and subsequently, seeded on the culture plate and maintained at 37 °C in a humidified incubator containing 5% CO_2.

Lentivirus packaging

Single guide RNAs (sgRNAs) targeting mouse Sqle (sgRNA1, CCGCTGTCGCCATCGACACGGGG; sgRNA2, CGTGCTGGTGTTCCTGTCGCTGG), human SQLE (sgRNA1, CGTGCTGGTGTTCCTCTCGCTGG; sgRNA2, CCGCTGTCGCCACCGAAACGGGG), or human DHCR24 (sgRNA1,

GTCATCAAGCTCAGGCAACA; sgRNA2, GCAAGACCTTCATGTGCACG) were cloned into pLenti-CRISPR v2 vector. The full-length open reading frame of human SQLE (NM_003129.4), mouse Sqle (NM_009270), or human DHCR24 (NM_014762.4) was cloned into pCDH-CMV-MCS-EF1-Puro vector. For lentivirus packaging, 6 μg of plasmid DNA, 4.5 μg of psPAX2 (Addgene), 1.5 μg of pMD2.G (Addgene), and 30 μl of lipofectamine 2000 (Invitrogen) were mixed in 1.5 ml Opti-MEM (Gibco) and added into the 293T cells in a 10 cm culture dish. The medium was changed at 6 h post-transfection, and the culture supernatant was collected at 48 h after transfection.

RNA extraction and real-time quantitative PCR

Total RNA was extracted using TRIzol reagent (Invitrogen). Subsequently, complementary DNA (cDNA) was synthesized from a total of 1 μg RNA using RT reagent kit (TaKaRa). Real-time PCR was conducted using aliquots of cDNA and SYBR Green PCR Master Mix (Applied Biosystems) on a LightCycler 480 real-time PCR system (Roche). All reactions were performed in triplicate. β-actin was used as an internal control. 2^(-ΔΔCt) method was applied to calculate the fold change of the target gene expression. Primers used are listed in table S2.

Western blot analysis

Total protein was resolved by 10% SDS-polyacrylamide gel electrophoresis (SDS-PAGE) and transferred onto polyvinylidene fluoride membrane. After blocking with 5% skim milk (Sigma-Aldrich) for 1 h at room temperature, the membrane was incubated with primary antibodies (table S1) overnight at 4 °C followed by the secondary antibody for 1 h at room temperature. The proteins of interest were detected using ECL Western Blotting Substrates (Bio-Rad).

Cholesterol/ cholesteryl ester concentration measurement

Free cholesterol and cholesteryl ester contents of cell culture supernatants and mouse tumor tissues were measured using the Cholesterol/ Cholesteryl Ester Quantification Assay kit (Abcam) according to the manufacturer's instructions. Lipoprotein cholesterol concentrations were measured using the Cholesterol Assay Kit-HDL and LDL/VLDL (Abcam) according to the manufacturer's instructions.

Cytokine antibody array and ELISA determination of TGF-β2

The conditioned medium of HKCI2 with or without SQLE knockout was collected after 48 h culture, filtered through a 0.22 μm strainer, and analyzed with Human Cytokine Antibody Array (Membrane, 80 Targets; Abcam) following the manufacturer's instructions. Signal intensity of each spot was measured with Image Lab software (Bio-Rad) and normalized by six positive control intensities on each membrane.

The concentrations of human TGF-β2 in cell culture conditioned medium were measured with Human TGF-beta2 Quantikine ELISA Kit (R&D Systems). Mouse TGF-β2 in the serum and tumor lysates was determined by Mouse/Rat/Canine/Porcine TGF-beta2 Quantikine ELISA Kit (R&D Systems). TGF-beta2 Antibody and Recombinant Human TGF-beta2 Protein (R&D Systems) were used in T cell co-culture assays *in vitro*.

Serum AFP measurement

Serum AFP levels of WT and *Sqle* tg or knockout mice were detected using the mouse AFP Quantikine ELISA kit (R&D Systems) according to the manufacturer's instructions.

Analysis of the Cancer Genome Atlas (TCGA)-Liver Hepatocellular Carcinoma dataset

The overall survival of HCC patients in relation to SQLE expression was assessed by the Kaplan-Meier survival curve and the log-rank test using KM Plotter[3]. The correlation between SQLE expression and MDSC infiltration or GZMB expression was evaluated with the Spearman's correlation coefficient Rho using TIMER 2.0[4].

References

1. Xu W, Zhang X, Wu JL, et al. O-GlcNAc transferase promotes fatty liver-associated liver cancer through inducing palmitic acid and activating endoplasmic reticulum stress. J Hepatol 2017;67:310-320.
2. Eggert T, Wolter K, Ji J, et al. Distinct Functions of Senescence-Associated Immune Responses in Liver Tumor Surveillance and Tumor Progression. Cancer Cell 2016;30:533-547.
3. Menyhárt O, Nagy Á, Győrffy B. Determining consistent prognostic biomarkers of overall survival and vascular invasion in hepatocellular carcinoma. R Soc Open Sci 2018;5:181006.
4. Li T, Fu J, Zeng Z, et al. TIMER2.0 for analysis of tumor-infiltrating immune cells. Nucleic Acids Res 2020;48:W509-w514.

Table S1. Antibodies used in this study

Antibodies	Source	Cat #
Brilliant Violet 605™ anti-mouse CD45 Antibody	Biolegend	103140
PE anti-mouse CD3 Antibody	Biolegend	100206
PE/Cyanine7 anti-mouse CD4 Antibody	Biolegend	100528
Brilliant Violet 711™ anti-mouse CD8a Antibody	Biolegend	100759
PE/Cyanine5 anti-mouse NK-1.1 Antibody	Biolegend	108716
Brilliant Violet 421™ anti-mouse CD279 (PD-1) Antibody	Biolegend	135221
FITC anti-mouse/human CD11b Antibody	Biolegend	101206
PE/Cyanine5 anti-mouse Ly-6G/Ly-6C (Gr-1) Antibody	Biolegend	108410
PE/Cyanine7 anti-mouse Ly-6G Antibody	Biolegend	127618
Brilliant Violet 421™ anti-mouse Ly-6C Antibody	Biolegend	128032
Arginase 1 Monoclonal Antibody (A1exF5), PE	eBioscience	12-3697-82
Arginase 1 Monoclonal Antibody (A1exF5), PE-Cyanine7	eBioscience	25-3697-82
PE/Cyanine5 anti-mouse F4/80 Antibody	Biolegend	123112
PE anti-mouse/human CD11b Antibody	Biolegend	101208
PE/Cyanine7 anti-mouse CD11c Antibody	Biolegend	117318
Brilliant Violet 421™ anti-mouse I-A/I-E Antibody	Biolegend	107632
Brilliant Violet 711™ anti-mouse CD206 (MMR) Antibody	Biolegend	141727
PE/Cyanine5 anti-mouse CD8a Antibody	Biolegend	100710
FITC anti-mouse TNF-α Antibody	Biolegend	506304
Brilliant Violet 421™ anti-mouse TNF-α Antibody	Biolegend	506328
Brilliant Violet 711™ anti-mouse IFN-γ Antibody	Biolegend	505836
Granzyme B Monoclonal Antibody (NGZB), PE-Cyanine7	eBioscience	25-8898-82
FITC anti-mouse CD3 Antibody	Biolegend	100203
PE anti-mouse CD186 (CXCR6) Antibody	Biolegend	151104

Purified anti-mouse CD16/32 Antibody	Biolegend	101302
APC/Cyanine7 anti-mouse CD45 Antibody	Biolegend	103116
FITC anti-mouse CD4 Antibody	Biolegend	100510
PerCP/Cyanine5.5 anti-mouse CD8a Antibody	Biolegend	100734
APC anti-mouse NK-1.1 Antibody	Biolegend	108709
Brilliant Violet 510™ anti-mouse CD19 Antibody	Biolegend	115546
Brilliant Violet 421™ anti-mouse Ly-6G/Ly-6C (Gr-1) Antibody	Biolegend	108445
FITC anti-mouse Ly-6G Antibody	Biolegend	127606
PerCP/Cyanine5.5 anti-mouse Ly-6C Antibody	Biolegend	128011
Arginase 1 Monoclonal Antibody (A1exF5), APC	eBioscience	17-3697-82
FITC anti-mouse F4/80 Antibody	Biolegend	123108
PerCP/Cyanine5.5 anti-mouse CD206 (MMR) Antibody	Biolegend	141715
APC anti-mouse CD11c Antibody	Biolegend	117309
Brilliant Violet 510™ anti-mouse TNF-α Antibody	Biolegend	506339
APC anti-mouse IFN-γ Antibody	Biolegend	505809
FITC anti-human/mouse Granzyme B Antibody	Biolegend	515403
SQLE Polyclonal antibody	Proteintech	12544-1-AP
β-Actin (13E5) Rabbit mAb	Cell Signaling	4970
Anti-DHCR7 antibody	Abcam	ab103296
DHCR24 Polyclonal antibody	Proteintech	10471-1-AP
LSS Polyclonal antibody	Proteintech	13715-1-AP
TGF-beta 2 Antibody	R&D Systems	AB-12-NA
InVivoPlus anti-mouse PD-1 (CD279)	BioXCell	BP0146
InVivoPlus rat IgG2a isotype control, anti-trinitrophenol	BioXCell	BP0089
InVivoMAb anti-mouse CD8α	BioXCell	BE0061
InVivoMAb rat IgG2b isotype control, anti-keyhole limpet hemocyanin	BioXCell	BE0090

InVivoMAb anti-mouse Ly6G/Ly6C (Gr-1)	BioXCell	BE0075

Table S2. Primer sequences

Primer name		Sequences
Arg1	Forward	CCTTTCTCAAAAGGACAGCCTC
	Reverse	CAGACCGTGGGTTCTTCACA
Nos2 (iNOS)	Forward	TCTAGTGAAGCAAAGCCCAACA
	Reverse	CTCTCCACTGCCCCAGTTTT
Ido1	Forward	GATGTTCGAAAGGTGCTGCC
	Reverse	AGAAGCTGCGATTTCCACCA
Tgfb1	Forward	GATACGCCTGAGTGGCTGTC
	Reverse	GGGGCTGATCCCGTTGATT
Cd274 (Pdl1)	Forward	CCTCGCCTGCAGATAGTTCC
	Reverse	CCCAGTACACCACTAACGCA
S100a9	Forward	GATGGAGCGCAGCATAACCA
	Reverse	GTTTGTGTCCAGGTCCTCCAT